RSC Medicinal Chemistry

ROYAL SOCIETY OF CHEMISTRY

RESEARCH ARTICLE

View Article Online
View Journal | View Issue

Check for updates

Cite this: *RSC Med. Chem.*, 2024, **15**, 178

Discovery of imidazo[1,2-*b*]pyridazine-containing TAK1 kinase inhibitors with excellent activities against multiple myeloma†

Desmond Akwata,[a] Allison L. Kempen,[a] Jones Lamptey,[a] Neetu Dayal,[a] Nickolas R. Brauer[a] and Herman O. Sintim*[abc]

Current treatment options for patients with multiple myeloma (MM) include proteasome inhibitors, anti-CD38 antibodies, and immunomodulatory agents. However, if patients have continued disease progression after administration of these treatments, there are limited options. There is a need for effective targeted therapies of MM. Recent studies have shown that the transforming growth factor-β activated kinase (TAK1) is upregulated and overexpressed in MM. We have discovered that 6-substituted morpholine or piperazine imidazo[1,2-*b*]pyridazines, with an appropriate aryl substituent at position-3, inhibit TAK1 at nanomolar concentrations. The lead compound, **26**, inhibits the enzymatic activity of TAK1 with an IC_{50} of 55 nM. Under similar conditions, the known TAK1 inhibitor, takinib, inhibits the kinase with an IC_{50} of 187 nM. Compound **26** and analogs thereof inhibit the growth of multiple myeloma cell lines MPC-11 and H929 with GI_{50} values as low as 30 nM. These compounds have the potential to be translated into anti-MM therapeutics.

Received 16th August 2023,
Accepted 7th November 2023

DOI: 10.1039/d3md00415e

rsc.li/medchem

Open Access Article. Published on 28 November 2023. Downloaded on 5/11/2024 5:37:14 AM.
This article is licensed under a Creative Commons Attribution-NonCommercial 3.0 Unported Licence.

Introduction

Multiple myeloma (MM), a blood cancer, is characterized by dysregulated and proliferative plasma cells, which facilitate bone destruction.[1–6] MM cells suppress the differentiation of osteoblasts from bone marrow stroma cells (BMSCs) and enhance osteoclastic formation and activity.[5–7] This process creates an imbalance leading to extensive bone damage and enhanced angiogenesis. MM cells have been found to overexpress several soluble inhibitors of osteoblastogenesis, including transforming growth factor-beta (TGF-β), tumor necrosis factor-alpha (TNF-α), interleukin-3 (IL-3), interleukin-7 (IL-7), and activin.[7]

Previous studies showed that the transforming growth factor-β activated kinase (TAK1) is constitutively upregulated and phosphorylated in MM.[1,6,8] TAK1 is a serine/threonine kinase that is important for cell growth, differentiation, and apoptosis.[8–10] Various extracellular signals trigger TAK1 activation, including cytokines, growth factors, and Toll-like receptor ligands. In the classical TAK1 signaling pathways, TAK1 is activated by receptor-associated proteins, such as TGF-β receptors or interleukin-1 receptors. Activation of these receptors recruits TAB1 and TAB2/3 to TAK1. TAK1 then phosphorylates downstream signaling molecules, including MAP kinases and various transcription factors.[11–15] TAK1 is involved in numerous cellular processes, including the regulation of immune responses, inflammation, cell survival, and differentiation.[15] Dysregulation of TAK1 has been implicated in various diseases, including cancer, autoimmune disorders, and inflammatory diseases.[15] Therefore, TAK1 has emerged as a potential target for therapeutic intervention in these diseases.

Overexpression of TAK1 has been found in many multiple myeloma cell lines as well as patient samples, suggesting that it may play a role in the development and progression of this disease.[16–19] Several studies have investigated the role of TAK1 in multiple myeloma. For example, a study by Teramachi *et al.* has shown that TAK1 is consistently upregulated and phosphorylated in MM cells. They found that inhibition of TAK1 leads to the suppression of NF-κB, p38MAPK, ERK, and STAT3 signaling pathways, which consequently inhibits the expression of key regulators involved in the growth and survival of MM, such as PIM2, MYC, Mcl1, IRF4, and Sp1. They also found that TAK1 inhibition significantly reduces the levels of the angiogenic factor VEGF in MM cells.[20] Another study by Harada *et al.* in 2021 highlighted that the dysregulation of the TAK1-PIM2 pathway is a key factor in promoting tumor growth and bone

[a] *Department of Chemistry, Purdue University, 560 Oval Drive, West Lafayette, IN 47907, USA. E-mail: hsintim@purdue.edu*
[b] *Purdue Institute for Drug Discovery, 720 Clinic Drive, West Lafayette, IN 47907, USA*
[c] *Purdue Institute for Cancer Research, 201 S. University St., West Lafayette, IN 47907, USA*

† Electronic supplementary information (ESI) available. See DOI: https://doi.org/10.1039/d3md00415e

This journal is © The Royal Society of Chemistry 2024

Open Access Article. Published on 28 November 2023. Downloaded on 5/11/2024 5:37:14 AM.
This article is licensed under a Creative Commons Attribution-NonCommercial 3.0 Unported Licence.

destruction in MM and that targeting the TAK1 pathway could be a therapeutic strategy for effectively addressing MM and its associated complications.[21] Overall, these findings suggest that TAK1 may be a promising therapeutic target for the treatment of multiple myeloma.

A few TAK1 inhibitors, such as OTS964, NG-25, LX-2343, 5Z-7-oxozeaenol, ponatinib, and takinib, have been described in the literature (Fig. 1).[22,23] Unfortunately, the reported GI_{50} values for these compounds against TAK1 overexpressing cancers, such as MM, are in the micromolar range and, as such, it would be difficult to achieve effective concentrations in blood without encountering dose-limiting toxicities.[24] Here, we present new and potent inhibitors of TAK1, which inhibit MM cell growth in the nanomolar range.

Results and discussion

The imidazo[1,2-*b*]pyridazine moiety is a privileged drug moiety that is found in many approved and experimental drugs.[24] It has been demonstrated in multiple reports that while the imidazo[1,2-*b*]pyridazine moiety binds to the hinge region of kinases, substitutions at positions 2, 3, 6, 7, and 8 dictate kinase selectivity and potency.[24] During a different project, we discovered that substituting position 6 of imidazo[1,2-*b*] pyridazine with morpholine or piperazine afforded compounds that displayed enhanced kinase inhibition when compared to analogs that were not substituted at position C6 of the imidazo[1,2-*b*]pyridazine core. We chose morpholine and piperazine because these moieties are known to enhance the drug-like properties of lead compounds and could also partake in ligand interactions with target proteins.[25,26] We designed compounds that fused the morpholine or piperazine imidazo[1,2-*b*]pyridazine scaffold with indazole (another privileged kinase scaffold), see Fig. 2 for structures. We initially synthesized a small set of such compounds with the imidazo[1,2-*b*]pyridazine as the main scaffold for a preliminary kinase screening. Compounds within this library were synthesized through a nucleophilic aromatic substitution (S_NAr) reaction at the C6 position. The final products were obtained by performing a Suzuki–Miyaura cross-coupling reaction with aromatic boronic acid substrates. This reaction was carried out using potassium carbonate as a base, a palladium catalyst, and a solvent mixture of acetonitrile and water in a 3 : 1 ratio (Scheme 1).

To evaluate the impact of substitution at C6 of the imidazo[1,2-*b*]pyridazine core, we synthesized compound **1**, allowing us to compare the differences between a substituted and unsubstituted structure at the C6 position. With the initial set of compounds on hand (Fig. 2), we began a kinase screening of the compounds at 100 nM against TAK1 utilizing the ADP-Glo kinase assay (Promega, Madison, WI).[27] Our preliminary data suggested that compound **3**, containing a *cis*-dimethylmorpholine moiety, showed the best inhibition of TAK1 (95%) compared to no substituent (**1**, 26% inhibition), the unsubstituted morpholine moiety (**2**, 91% inhibition), or the piperidine substituent (**4**, 46% inhibition). Thus, we decided to move forward with a structure–activity relationship (SAR) study based on compound **3**.

To investigate the potential binding mode of our preliminary compounds, we performed molecular docking studies of compound **3** and takinib against TAK1 (Fig. 3). We

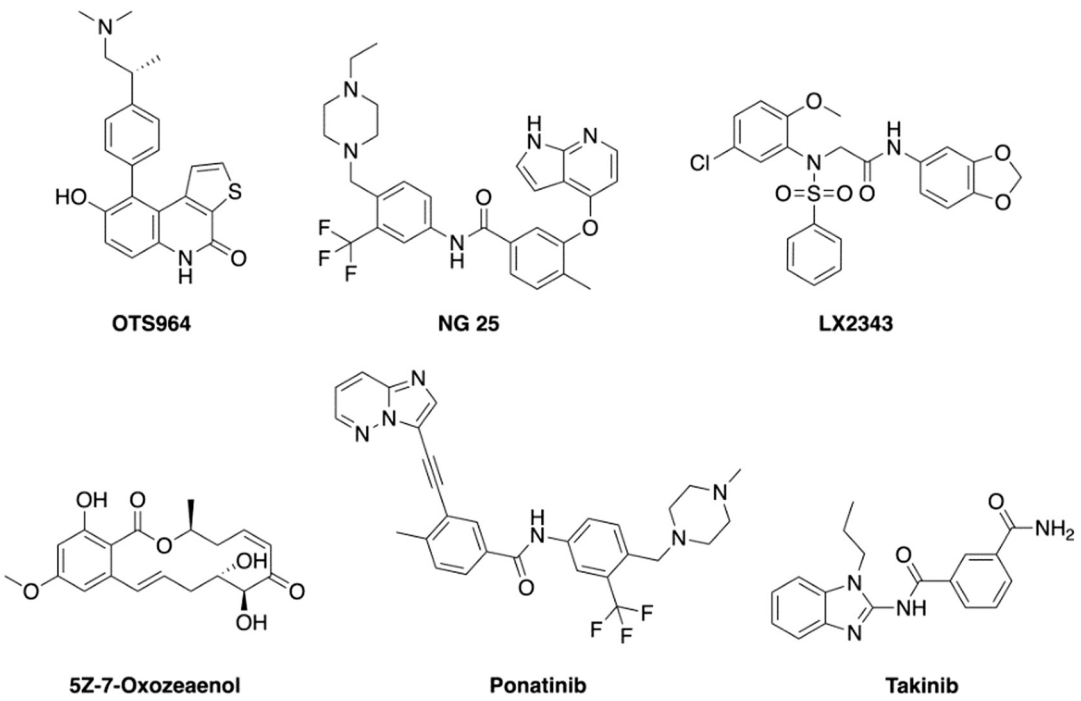

Fig. 1 Structures of reported small molecule TAK1 inhibitors.

Open Access Article. Published on 28 November 2023. Downloaded on 5/11/2024 5:37:14 AM.
This article is licensed under a Creative Commons Attribution-NonCommercial 3.0 Unported Licence.

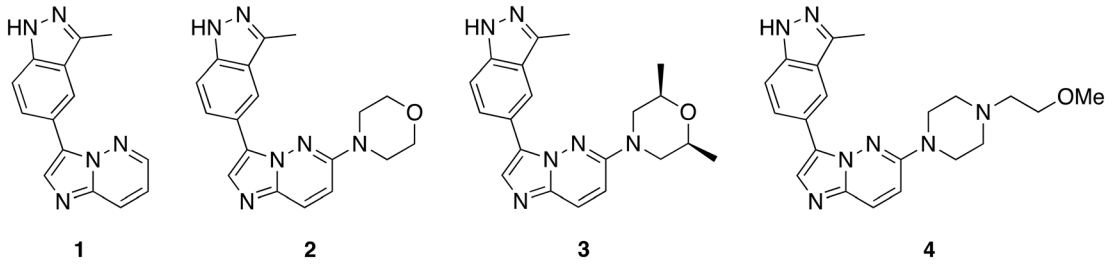

Fig. 2 Preliminary compounds synthesized and screened against TAK1.

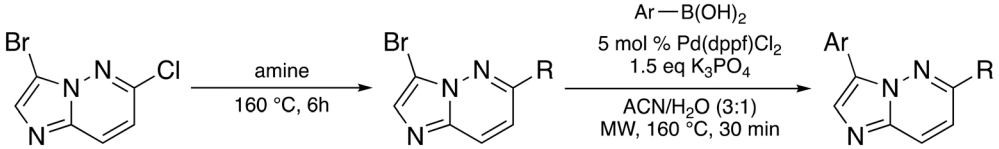

Scheme 1 Synthesis of compounds *via* nucleophilic aromatic substitution and Suzuki–Miyaura cross-coupling reaction.

found that the oxygen in the *cis*-dimethylmorpholine interacts with the conserved lysine residue Lys-63 in the ATP-binding site of TAK1 (Fig. 3), which is crucial for kinase activity as observed in the kinase inhibition data for **2** and **3**. The methyl groups of the morpholine formed favorable hydrophobic interactions with the surrounding residues, Cys-174, Lys-63, and Gly-45. In addition, we identified a hydrogen bonding interaction between Ala-107 and H2 of the imidazo[1,2-*b*]pyridazine core. We therefore hypothesized that blocking this position with a methyl group at position 2 of the imidazo[1,2-*b*]pyridazine (as in **28**) would sterically hinder this hydrogen bonding and lead to reduced activity, *vide infra*.

We synthesized three types of compound **3** analogs, where series A explores the use of phenyl derivatives in place of the indazole, series B examines indazole derivatives, and series C evaluates the effect of modifying the morpholine moiety.

In series A (Fig. 4), we probed the use of substituted phenyls and pyridine rings in place of the indazole as found in compound **3**. Specifically, we synthesized compounds with privileged moieties, such as halides, $-OCF_3$, –CN, and $-CF_3$ at the C3 position. These groups are known to enhance the potency of a drug by increasing its binding affinity to the target protein and improve the pharmacokinetic properties of a drug by increasing its lipophilicity, which can enhance its membrane permeability and metabolic stability.[28,29] We explored the use of a pyridine ring (**17** and **18**) as a bioisostere of phenyl (as in **5**). The so-called "necessary nitrogen" scanning (for example phenyl to pyridyl) could enhance solubility and/or activity of a lead compound *via* hydrogen bonding and polar interactions with water and/or active site residues.[30] Additionally, we tested substituents such as amides on the phenyl (**12** and **13**) as their polarity, electron-withdrawing capability, and hydrogen-bonding ability are known to improve the potency and selectivity of a drug by enhancing its binding affinity to the target protein or receptor. Compounds **8** and **15** were made with sulfonyl and sulfonamide groups, which can enhance the metabolic stability of drugs (compared to amides) by resisting enzymatic degradation.[31,32]

We went on to explore different indazole derivatives in series B (Fig. 5). In this series, we synthesized analogs with different indazole derivatives attached to the imidazo[1,2-*b*]pyridazine core scaffold at positions 4, 5, and 7 of the indazole (**20**, **21**, and **22**). We also synthesized methylated analogs (**23** and **24**) at the 1*H*-position of compounds **21** and **20**, respectively. Based on the activity of **3**, we synthesized **25** and **26**, to investigate how different alkyl groups on the indazole moiety affected kinase activity. **27** substitutes an indolin-2-one as a bioisostere of indazole. The introduction of different indazole derivatives/mimics at the C3 position of the imidazo[1,2-*b*]pyridazine scaffold was expected to modulate the steric and electronic properties of the molecule, which in turn could affect its interactions with the target protein kinase.

The introduction of morpholine at C6 of the imidazo[1,2-*b*]pyridazine core improved TAK1 kinase inhibition when compared to **1**, which has no substitution at C6, and **4**, which has a piperazine moiety at C6. For series C, we made analogs of **3** exploring the substitution of different substituted morpholine moieties at the C6 position (Fig. 6). Morpholines in drugs are known to enhance the water solubility and metabolic stability of a drug and improve its bioavailability.[33] Morpholines can also be used to enhance the receptor binding affinity of a drug by engaging in additional hydrogen-bonding interactions with the protein target. This can improve the potency and the selectivity of the drug, as well as reduce its off-target effects.[33–35] As the *cis*-dimethylmorpholine analog showed higher inhibition compared to the unsubstituted morpholine (**2**), we made analogs of **3** exploring the substitution of different substituted morpholines at the C6 position (Fig. 6).

 This journal is © The Royal Society of Chemistry 2024

Open Access Article. Published on 28 November 2023. Downloaded on 5/11/2024 5:37:14 AM.
This article is licensed under a Creative Commons Attribution-NonCommercial 3.0 Unported Licence.

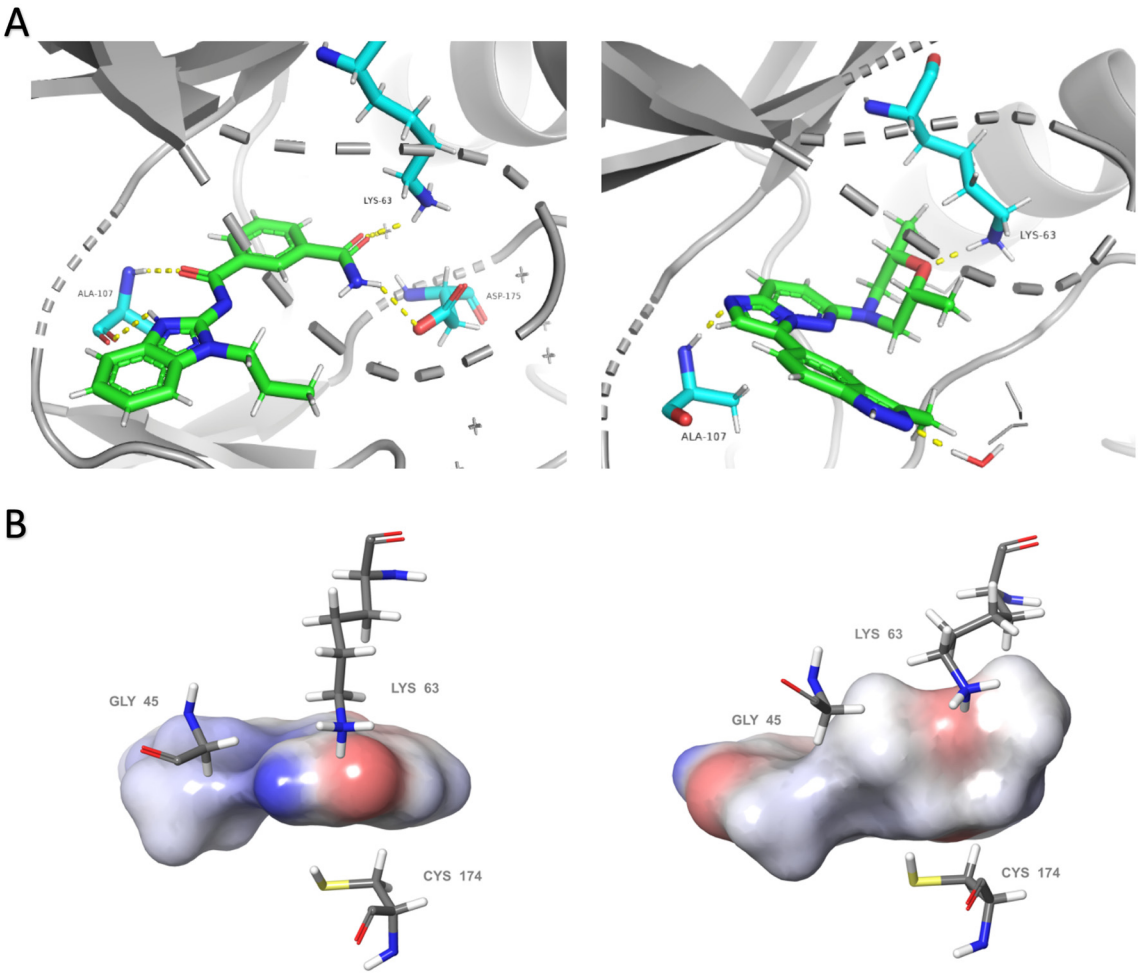

Fig. 3 Comparative analysis of binding modes of takinib and docking model of compound **3** within the binding pocket of TAK1 (PDB: 5V5N). (A) Polar interactions (yellow dashes) between takinib (left) and compound **3** (right) and active site of TAK1. Each ligand forms hydrogen bonds with the conserved lysine Lys-63 and with Ala-107 within the hinge region. Takinib makes an additional interaction with DFG residue Asp-175. (B) Surface models of each ligand surrounded by representative hydrophobic residues within the binding pocket. Slight conformational shifts to residues Lys-63, Gly-45, and Cys-174 from the bound structure of takinib to the docked structure of compound **3** indicate a possible induction of entropically favored hydrophobic interactions. Docking was performed using the Induced Fit Docking protocol within Schrodinger. Visualization of (A) was performed in PyMol. Visualization of (B) utilized Maestro.

With the library on hand, we screened the compounds against TAK1 using the ADP-Glo kinase assay (Promega, Madison, WI) at a compound concentration of 500 nM (Fig. 7). We identified the best-performing compounds that exhibited over 50% inhibition at 500 nM. Then, we subjected these compounds to further screening at a concentration of 100 nM. We then conducted a final screening of the remaining compounds, which had >50% inhibition at 100 nM, at a concentration of 20 nM (Fig. 7).

To evaluate the significance of kinase inhibition, a cutoff value of 50% was used to classify compounds as having good kinase inhibition or not. At 500 nM screening, 16 compounds out of the 35 demonstrated good kinase inhibition, surpassing the 50% cutoff. Notably, compounds **3**, **25**, **26**, **31**, and **33** exhibited exceptional potency, achieving 100% kinase inhibition. Conversely, all the compounds in series A apart from **12** (74%) showed less than 50% kinase inhibition, with **6**, **7**, **8**, **9**, **13**, **14**, **16**, and **17** showing moderate kinase inhibition. Compounds **5**, **11**, **18**, and **19** exhibited negligible kinase inhibition. Additionally, compounds **21**, **22**, **24**, **27**, and **28** in series B also showed moderate kinase inhibition below the 50% cutoff. These compounds may not effectively target the kinase of interest but may still have some inhibitory potential with further modifications. The compounds demonstrating kinase inhibition above 50% were subjected to a second round of screening at a lower concentration of 100 nM.

Comparing the kinase inhibition at 100 nM to the previous screening at 500 nM, some compounds show consistent inhibition, while others demonstrate variations in their inhibitory activities. Notably, compounds **2**, **3**, **25**, **26**, **31**, **32**, **33**, and **35** continue to exhibit significant TAK1 kinase inhibition above the 50% cutoff, indicating their consistent inhibitory potential. Compounds **4** and **12** show a decrease in

Open Access Article. Published on 28 November 2023. Downloaded on 5/11/2024 5:37:14 AM.
This article is licensed under a Creative Commons Attribution-NonCommercial 3.0 Unported Licence.

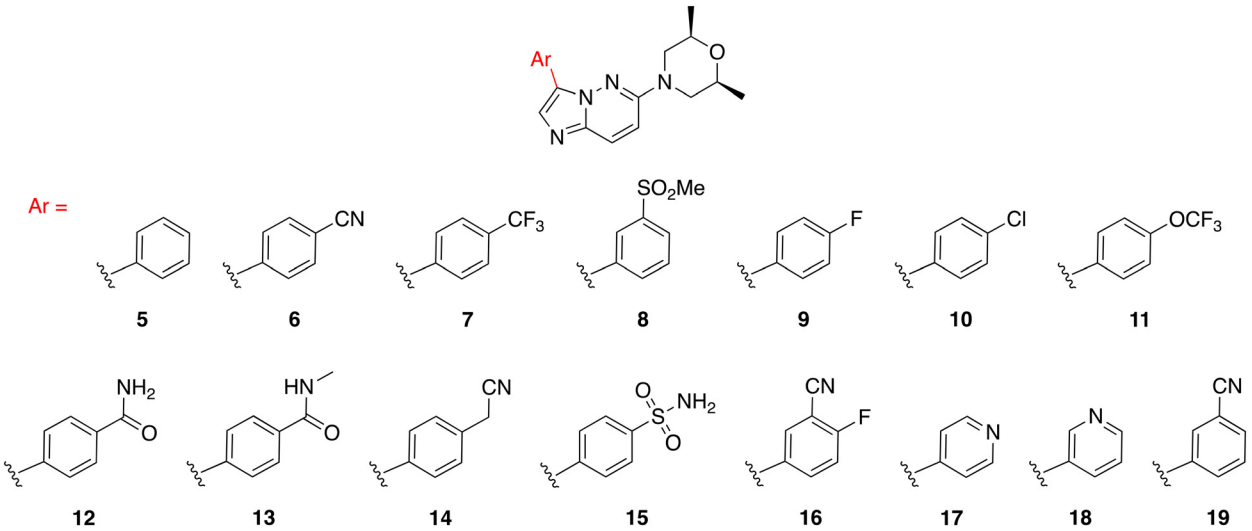

Fig. 4 Series A: analogs of **3** with different 6-membered ring substitutions at position C3.

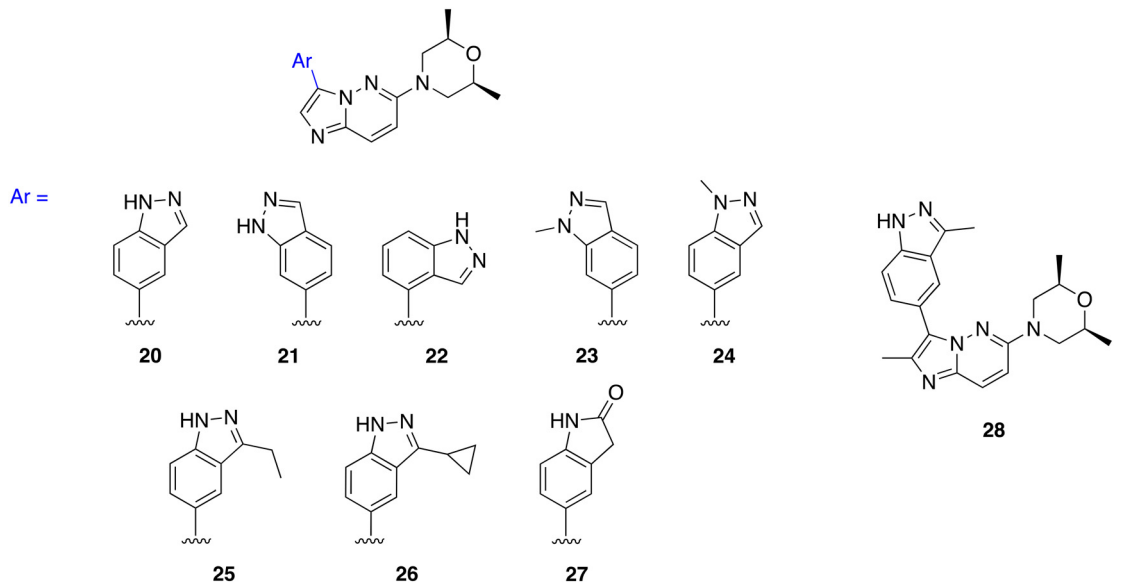

Fig. 5 Series B: analogs of **3** with various indazole derivatives.

TAK1 kinase inhibition compared to the previous screening, suggesting a potential concentration-dependent effect. Again, all compounds in series C (**29–35**) exhibited excellent TAK1 kinase inhibition.

To confirm our in-house kinase assay results, an enzymatic IC_{50} assay was performed on the top ten compounds, with takinib used as a control, at a contract research service company (Reaction Biology). The results showed that compound **26** was the most potent TAK1 inhibitor, with an IC_{50} value of 55 nM; under similar experimental conditions, the IC_{50} for the known TAK1 inhibitor, takinib, was 187 nM. Additionally, six of the ten analogs tested also had a lower IC_{50} than takinib (Fig. 8).

As stated earlier, studies have shown that TAK1 is overexpressed in many multiple myeloma cells. To investigate the performance of these compounds in cell culture, we explored the effect of the library on MM cell growth inhibition (Fig. 9). Compounds were screened at 1 and 0.2 μM against the MPC-11 cell line.

The compounds showed a relative consistency between activity against TAK1 and antiproliferative activity against multiple myeloma cells. All compounds in series C (**29–35**) showed excellent inhibitory activity against TAK1, and, with the exception of **33**, had significant cellular growth inhibition. It is interesting to note that **32** and **33** are enantiomers and show similar TAK1 inhibitions but display different cellular activities. Compound **32** inhibited ~50% of MPC-11 at 200 nM, while at the same concentration **33** was inactive. We do not have a hypothesis for this discrepancy but appreciate that before a compound can engage with cellular targets it has to get into the cell and differences in permeation and/or compound stability might account for

 This journal is © The Royal Society of Chemistry 2024

Open Access Article. Published on 28 November 2023. Downloaded on 5/11/2024 5:37:14 AM.
This article is licensed under a Creative Commons Attribution-NonCommercial 3.0 Unported Licence.

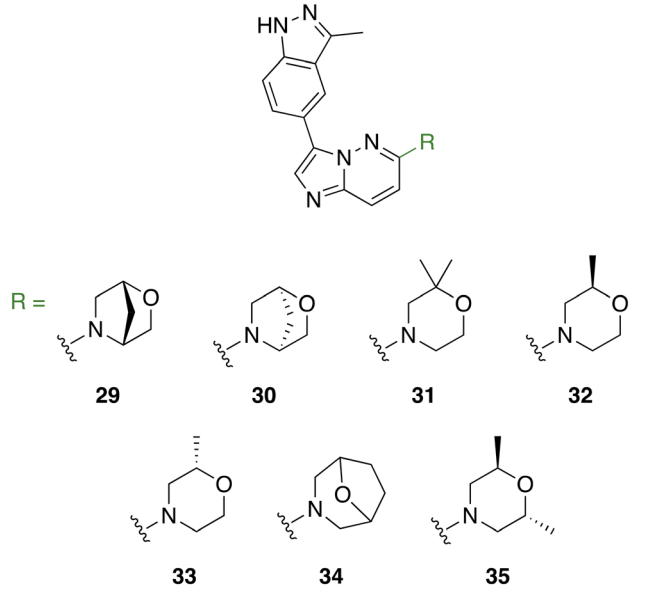

Fig. 6 Series C: analogs of **3** with different heterocyclic substitutions at position C6.

such differences. Nonetheless, because 2-oxa-5-azabicyclo[2.2.1]heptane, found in **32** or **33**, is not the best substituent, we did not expend our resources looking into the origin of differences between **32** and **33**.

Based on our cell growth inhibition results, we moved forward to collect GI_{50} values of the top compounds to evaluate their effectiveness (Table 1). We determined the GI_{50} values of these compounds against two distinct multiple myeloma (MM) cell lines: H929, a human plasma MM cell line, and MPC-11, a murine plasmacytoma cell line. Interestingly, our findings revealed that all the top compounds demonstrated remarkable potency against the H929 cells, with compound **31** exhibiting the most exceptional activity, recording a GI_{50} value of 0.024 μM (24 nM). Notably, the lead compounds **3** and **26** displayed GI_{50} values of 0.087 μM (87 nM) and 0.043 μM (43 nM), respectively, indicating their high efficacy against the H929 cells. In comparison, takinib, a known TAK1 inhibitor, exhibited a significantly higher GI_{50} value of 51 μM (51 000 nM), making it over 500 times less effective than the least active compound **3** (GI_{50} = 0.087 μM).

Similarly, the evaluation of these top compounds against the MPC-11 cells demonstrated promising results, with all compounds exhibiting favorable GI_{50} values ranging from 0.041 μM (**26**) to 0.155 μM (**29**). Once again, takinib proved to be substantially less potent with a GI_{50} value of 8.5 μM against the MPC-11 cells. These findings highlight the outstanding potential of our identified compounds as potent inhibitors against both human and murine MM cell lines. Notably, their efficacy against the H929 cells, particularly compound **31**, stands out as a highly promising avenue for further investigation (see ESI† Fig. S1 for dose–response curves).

TAK1 ser412 phosphorylation has been shown to be essential for regulation of downstream pathways by TAK1; the TAK1 S412A mutant could not support the activation of the p38, JNK, and NF-κB pathways.[36] Thus we wanted to know if our compounds could inhibit TAK1 phosphorylation at ser412 in murine MM MPC-11 cells (Fig. 10). The results showed that both compounds **3** and **26** were successful in reducing levels of phosphorylated TAK1 (S412) compared to the DMSO control. Treating with 0.5 μM compound decreased phosphorylation levels more significantly than treatment at 0.1 μM. Additionally, takinib did not show a significant difference in phosphorylated TAK1 (S412) levels at 0.1 or 0.5 μM.

Since compound **26** was effective in inhibiting TAK1 phosphorylation in cells, it was profiled against some essential kinases to determine potential liabilities, using Eurofins KinomeScan but displayed minimal inhibition of kinase anti-targets, which are essential kinases and/or kinases that are important for immune, kidney or cardiovascular or skin functions, such as KIT, ZAP70, JAK2, RET, KDR (VEGFR2), PDGFR, FGFR, EGFR, BRAF, AKT, AURKA or B (see the ESI,† Table S1). Interestingly, compound **26** showed low affinity for PKAC alpha[26] (ESI,† Table S1) and hence the inhibition of p-TAK1 (S412) is intriguing, which requires future investigation.

Conclusion

TAK1 is an important kinase that is involved in many critical processes and has been proposed as a potential target for various disease states, including cancer and inflammatory diseases. While a few TAK1 inhibitors have been reported, to the best of our knowledge, none has been shown to potently inhibit TAK1 phosphorylation or inhibit MM cell growth at low nanomolar concentrations. Here, we show that the strategic substitution of the imidazo[1,2-*b*]pyridazine core with morpholine and indazole affords excellent TAK1 inhibitors with activities against MM cell lines. We also utilize the so-called "magic methylation" on the morpholine ring to increase TAK1 inhibition.

Experimental

General procedure for the synthesis of substituted imidazo[1,2-*b*] pyridazine substrates

In a sealed tube, 3-bromo-6-chloroimidazo[1,2-*b*] pyridazine (500 mg) and appropriate amine (4 equiv.) in *n*-propanol (1 mL) was refluxed at 150 °C overnight. After completion, the reaction was extracted with ethyl acetate and washed with brine. The organic layer was collected, dried over sodium sulfate, and concentrated under reduced pressure. The crude was purified *via* silica gel column chromatography to yield the desired product.

Suzuki cross-coupling synthesis of compound 3 and analogs

A solution of (2*S*,6*R*)-4-(3-bromoimidazo[1,2-*b*] pyridazin-6-yl)-2,6-dimethyl morpholine (0.5 mmol), respective boronic acid substrates, $Pd(dppf)_2Cl_2$ (5 mol%), K_3PO_4 (1.5 equiv.) in degassed acetonitrile (3 mL) and water (1 mL) was stirred at 160 °C in a sealed microwave vial for 30 minutes in a

Open Access Article. Published on 28 November 2023. Downloaded on 5/11/2024 5:37:14 AM.
This article is licensed under a Creative Commons Attribution-NonCommercial 3.0 Unported Licence.

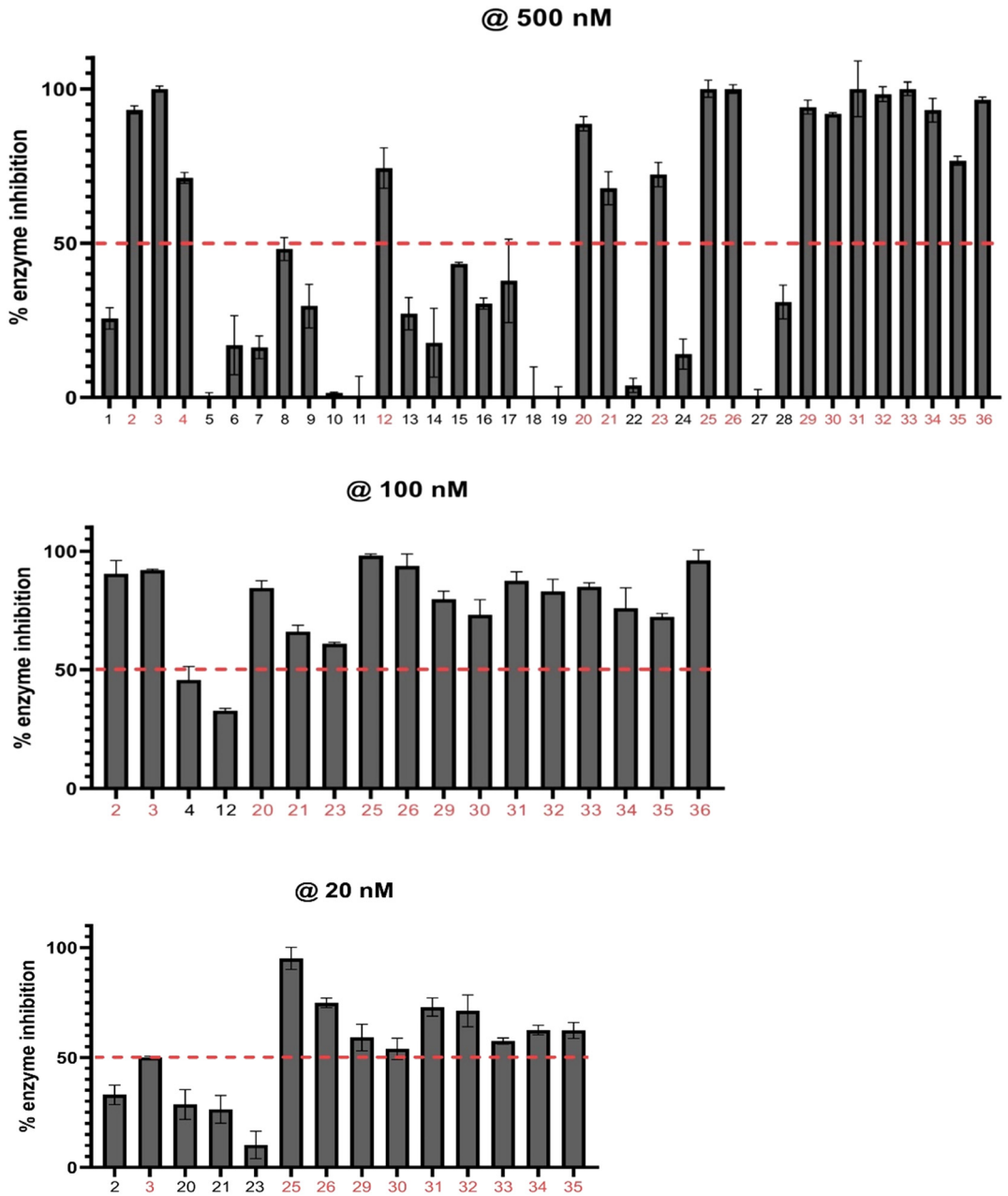

Fig. 7 Histograms of TAK1 inhibition at compound concentrations of 500 nM, 100 nM, and 20 nM. Compounds were screened against TAK1 using the ADP-Glo kinase assay (Promega). The dashed red line denotes 50% enzyme inhibition, and compounds performing above the line were assessed at the next concentration. Values reported represent means of triplicates, and error bars represent standard deviation.

microwave oven. The organic layer was collected after workup with water and ethyl acetate, and the organic layer was washed with brine, followed by concentration using a rotary evaporator and purification by silica gel column chromatography to obtain the final product.

3-(3-Methyl-1*H*-indazol-5-yl)imidazo[1,2-*b*]pyridazine (1)

Pale yellow solid (69 mg, 49%). ^{1}H NMR (500 MHz, methanol-d_4) δ 8.58–8.52 (m, 2H), 8.09 (s, 1H), 8.05 (dd, J = 9.2, 1.7 Hz, 1H),7.99 (dd, J = 8.8, 1.6 Hz, 1H), 7.55 (dd, J = 8.7, 0.9 Hz, 1H), 7.25 (dd, J = 9.2, 4.4 Hz, 1H), 2.60 (s, 3H). ^{13}C NMR (126 MHz, methanol-d_4) δ 143.5, 142.8, 140.6, 139.7, 130.9, 129.1, 126.2, 124.9, 122.2, 120.3, 118.4, 117.1, 110.0, 10.3. HRMS (ESI†) m/z calcd. for $C_{14}H_{11}N_5$ $[M+H]^+$ 250.1093, found 250.1090.

4-(3-Bromoimidazo[1,2-*b*]pyridazin-6-yl)morpholine (S1)

Brown solid (552 mg, 87%). ^{1}H NMR (500 MHz, methanol-d_4) δ 7.72 (d, J = 10.0 Hz, 1H), 7.50 (s, 1H), 7.15 (d, J = 10.0 Hz, 1H), 3.85–3.79 (m, 4H), 3.59–3.53 (m, 4H). ^{13}C NMR (126 MHz, methanol-d_4) δ 155.7, 136.9, 130.8, 124.9, 110.8, 100.2, 66.1,

 This journal is © The Royal Society of Chemistry 2024

Open Access Article. Published on 28 November 2023. Downloaded on 5/11/2024 5:37:14 AM.
This article is licensed under a Creative Commons Attribution-NonCommercial 3.0 Unported Licence.

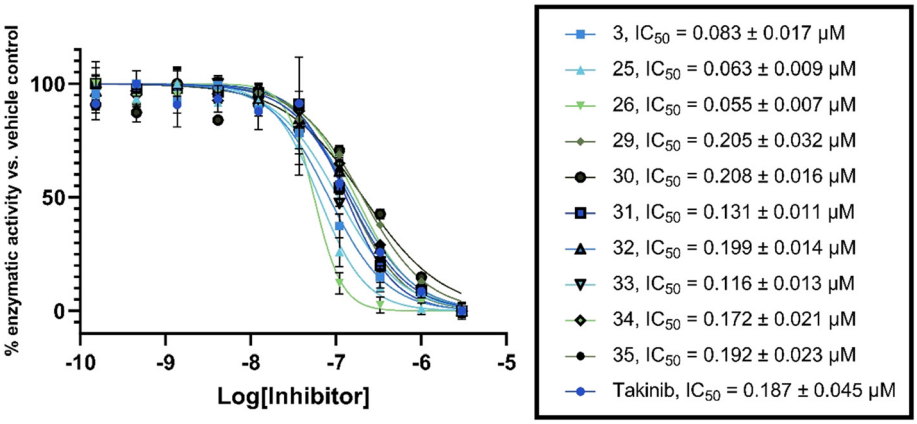

Fig. 8 TAK1 inhibition. IC_{50} values obtained by Reaction Biology. Data were fitted to a non-linear regression equation using GraphPad Prism 9.0 software. Each data point represents the mean and error bars represent the SD of duplicates.

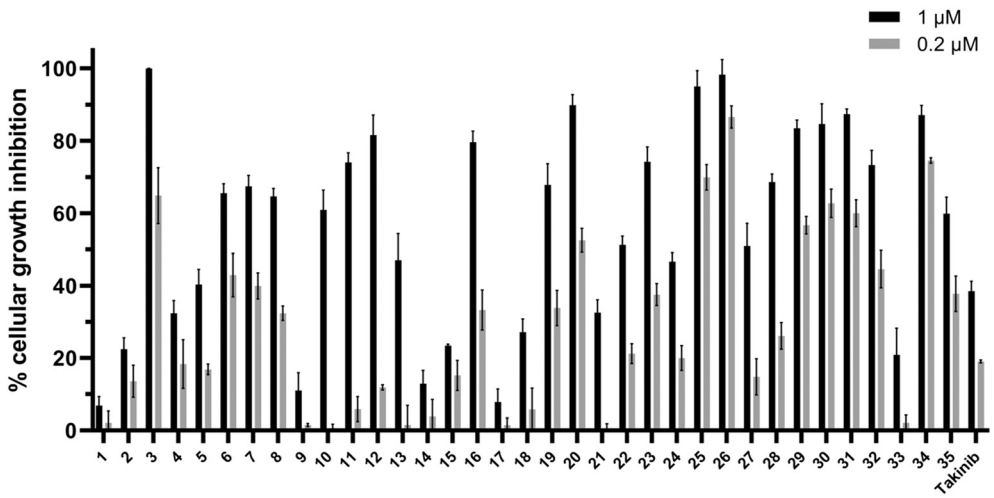

Fig. 9 Compounds (1 and 0.2 μM) against MPC-11 cells. Each data point represents the mean and error bars represent the SD of triplicates.

45.9. HRMS (ESI†) *m*/*z* calcd. for $C_{13}H_{14}N_6O$ $[M + H]^+$ 284.1311, found 284.1311.

4-(3-(3-Methyl-1*H*-indazol-5-yl)imidazo[1,2-*b*]pyridazin-6-yl) morpholine (2)

Synthesized using substrate **S1**. Brown solid (95 mg, 50%). ^{1}H NMR (500 MHz, methanol-d_4) δ 8.60–8.56 (m, 1H), 7.93 (dd, J = 8.8, 1.6 Hz, 1H), 7.84 (s, 1H), 7.75 (d, J = 9.9 Hz, 1H), 7.49 (dd, J = 8.8, 0.8 Hz, 1H), 7.09 (d, J = 9.9 Hz, 1H), 3.86–3.78 (m, 4H), 3.57–3.48 (m, 4H), 2.55 (d, J = 2.3 Hz, 3H). ^{13}C NMR (126 MHz, DMSO-d_6) δ 155.4, 142.2, 140.3, 137.3, 130.9, 128.0, 126.7, 125.3, 122.7, 121.0, 117.5, 110.7, 109.9, 66.2, 46.7, 12.1. HRMS (ESI†) *m*/*z* calcd. for $C_{18}H_{18}N_6O$ $[M + H]^+$ 335.1621, found 335.1621.

Table 1 GI_{50} of selected active compounds with takinib as a control drug treated against H929 cells and MPC-11 cells

Compound	H929 (GI_{50})	MPC-11 (GI_{50})
3	0.087 ± 0.024 μM	0.072 ± 0.011 μM
25	0.030 ± 0.006 μM	0.094 ± 0.023 μM
26	0.043 ± 0.014 μM	0.041 ± 0.012 μM
29	0.071 ± 0.012 μM	0.155 ± 0.019 μM
30	0.045 ± 0.009 μM	0.101 ± 0.015 μM
31	0.024 ± 0.005 μM	0.126 ± 0.028 μM
34	0.033 ± 0.008 μM	0.131 ± 0.026 μM
Takinib	51 ± 9 μM	8.5 ± 2.9 μM

(2*S*,6*R*)-4-(3-Bromoimidazo[1,2-b] pyridazin-6-yl)-2,6-dimethylmorpholine (S2)

Pale yellow solid (640 mg, 95%). ^{1}H NMR (500 MHz, chloroform-*d*) δ 7.66 (d, J = 9.9 Hz, 1H), 7.52 (s, 1H), 6.80 (d, J = 9.9 Hz, 1H), 4.01–3.89 (m, 2H), 3.81–3.65 (m, 2H), 2.65 (dd, J = 12.8, 10.6 Hz, 2H), 1.28 (d, J = 6.3 Hz, 6H). ^{13}C NMR (125 MHz, Chloroform-*d*) δ 154.8, 136.9, 132.1, 126.0, 109.4, 100.3, 71.3, 51.3, 18.9. HRMS (ESI†) *m*/*z* calcd. for $C_{12}H_{16}BrN_4O$ $[M + H]^+$ 311.0507, found 311.0507.

Open Access Article. Published on 28 November 2023. Downloaded on 5/11/2024 5:37:14 AM.
This article is licensed under a Creative Commons Attribution-NonCommercial 3.0 Unported Licence.

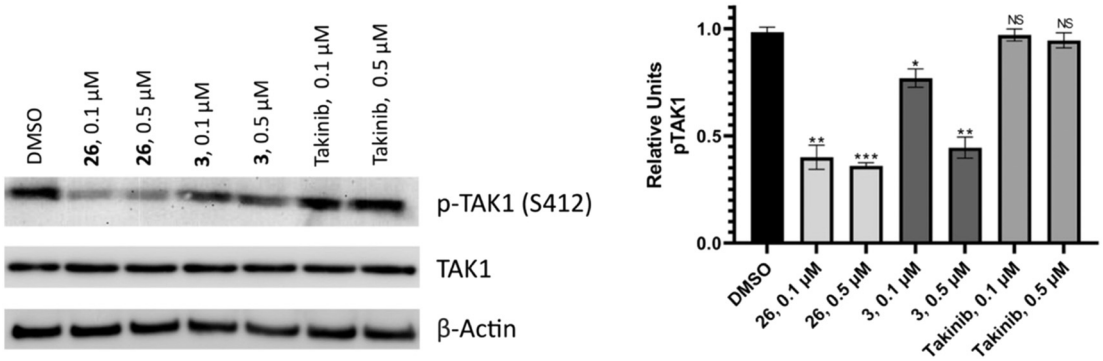

Fig. 10 Western blot analysis. MPC-11 cells were treated with compounds **26** or **3** at 0.1 or 0.5 μM or the DMSO control for 48 hours. Bands were quantified relative to the actin loading control. Values are reported as means of duplicates and error bars represent standard deviation.

(2*S*,6*R*)-2,6-Dimethyl-4-(3-(3-methyl-1*H*-indazol-5-yl) imidazo[1,2-*b*]pyridazin-6-yl)morpholine (3)

Synthesized using substrate **S2**. Off-white solid (142 mg, 42%). ^{1}H NMR (500 MHz, methanol-d_4) δ 8.69 (dd, J = 1.6, 0.8 Hz, 1H), 7.86 (dd, J = 8.8, 1.6 Hz, 1H), 7.84 (s, 1H), 7.69 (d, J = 9.8 Hz, 1H), 7.46 (dd, J = 8.8, 0.9 Hz, 1H), 7.06 (d, J = 10.0 Hz, 1H), 3.97–3.90 (m, 2H), 3.73 (dqd, J = 12.4, 6.2, 2.4 Hz, 2H), 2.57–2.51 (m, 2H), 2.51 (s, 3H), 1.22 (d, J = 6.3 Hz, 6H). ^{13}C NMR (126 MHz, methanol-d_4) δ 154.9, 142.5, 140.2, 137.0, 128.8, 128.2, 125.6, 124.8, 122.0, 121.0, 117.2, 109.9, 71.3, 51.4, 17.8, 10.5. HRMS (ESI†) m/z calcd. for $C_{20}H_{22}N_6O$ $[M + H]^+$ 363.1928, found 363.1939.

3-Bromo-6-(4-(2-methoxyethyl)piperazin-1-yl)imidazo[1,2-*b*] pyridazine (S3)

Off-white solid (583 mg, 79%). ^{1}H NMR (500 MHz, Methanol-d_4) δ 7.66 (d, J = 9.9 Hz, 1H), 7.47 (s, 1H), 7.10 (d, J = 10.0 Hz, 1H), 3.61–3.51 (m, 6H), 3.34 (s, 3H), 2.66–2.58 (m, 6H); ^{13}C NMR (125 MHz, Methanol-d_4) δ 155.3, 136.7, 130.6, 124.8, 110.9, 100.1, 69.6, 57.6, 57.2, 52.6, 45.1. HRMS (ESI†) m/z calcd. for $C_{13}H_{19}BrN_5O$ $[M + H]^+$ 340.0773, found 340.0770.

6-(4-(2-Methoxyethyl)piperazin-1-yl)-3-(3-methyl-1*H*-indazol-5-yl)imidazo[1,2-*b*]pyridazine (4)

Synthesized using substrate **S3**. Yellow solid (174 mg, 78%). ^{1}H NMR (500 MHz, methanol-d_4) δ 8.54 (dd, J = 1.6, 0.8 Hz, 1H), 7.86 (dd, J = 8.8, 1.6 Hz, 1H), 7.78 (s, 1H), 7.64 (d, J = 9.9 Hz, 1H), 7.44 (dd, J = 8.8, 0.9 Hz, 1H), 6.98 (d, J = 9.9 Hz, 1H), 3.55 (t, J = 5.5 Hz, 2H), 3.54–3.48 (m, 4H), 3.34 (s, 3H), 2.65–2.62 (m, 4H), 2.60 (d, J = 5.5 Hz, 2H), 2.50 (s, 3H). ^{13}C NMR (126 MHz, methanol-d_4) δ 154.8, 142.5, 140.2, 136.8, 128.8, 128.3, 125.6, 124.7, 122.0, 121.0, 117.4, 110.0, 109.9, 69.5, 57.6, 57.2, 52.6, 45.5, 10.3. HRMS (ESI†) m/z calcd. for $C_{21}H_{25}N_7O$ $[M + H]^+$ 392.2199, found 392.2202.

(2*S*,6*R*)-2,6-Dimethyl-4-(3-phenylimidazo[1,2-*b*]pyridazin-6-yl) morpholine (5)

Synthesized using substrate **S2**. Off-white solid (241 mg, 81%). ^{1}H NMR (500 MHz, methanol-d_4) δ 8.05 (dd, J = 8.4, 1.2 Hz, 2H), 7.80 (s, 1H), 7.72 (d, J = 9.9 Hz, 1H), 7.44 (dd, J = 8.5, 7.1 Hz, 2H), 7.36–7.29 (m, 1H), 7.11 (d, J = 10.0 Hz, 1H), 4.01–3.94 (m, 2H), 3.72 (dqd, J = 10.6, 6.2, 2.4 Hz, 2H), 2.57 (dd, J = 12.9, 10.6 Hz, 2H), 1.22 (d, J = 6.3 Hz, 6H). ^{13}C NMR (126 MHz, methanol-d_4) δ 154.8, 137.1, 129.4, 128.9, 128.2, 128.2, 127.3, 126.2, 125.0, 110.5, 71.2, 51.4, 17.7. HRMS (ESI†) m/z calcd. for $C_{18}H_{20}N_4O$ $[M+H]^+$ 309.1715, found 309.1718.

4-(6-((2*S*,6*R*)-2,6-Dimethylmorpholino)imidazo[1,2-*b*] pyridazin-3-yl)benzonitrile (6)

Synthesized using substrate **S2**. Off-white solid (246 mg, 77%). ^{1}H NMR (500 MHz, methanol-d_4) δ 8.32–8.25 (m, 2H), 7.99 (s, 1H), 7.78 (dd, J = 9.3, 8.4 Hz, 3H), 7.22 (d, J = 10.0 Hz, 1H), 4.05–3.98 (m, 2H), 3.76 (dqd, J = 12.6, 6.2, 2.4 Hz, 2H), 2.63 (dd, J = 12.8, 10.6 Hz, 2H), 1.26 (d, J = 6.2 Hz, 6H). ^{13}C NMR (126 MHz, methanol-d_4) δ 155.1, 138.1, 133.5, 132.1, 131.2, 126.2, 126.0, 125.2, 118.4, 111.5, 109.9, 71.3, 51.3, 17.7. HRMS (ESI†) m/z calcd. for $C_{19}H_{19}N_5O$ $[M+H]^+$ 334.1668, found 334.1671.

(2*S*,6*R*)-2,6-Dimethyl-4-(3-(4-(trifluoromethyl)phenyl) imidazo[1,2-b]pyridazin-6-yl)morpholine (7)

Synthesized using substrate **S2**. Pale yellow solid (248 mg, 68%). ^{1}H NMR (500 MHz, methanol-d_4) δ 8.34–8.28 (m, 2H), 7.97 (s, 1H), 7.81 (d, J = 9.9 Hz, 1H), 7.78–7.72 (m, 2H), 7.23 (d, J = 10.0 Hz, 1H), 4.04 (ddd, J = 12.0, 2.3, 1.0 Hz, 2H), 3.78 (dqd, J = 10.5, 6.2, 2.4 Hz, 2H), 2.65 (dd, J = 12.9, 10.6 Hz, 2H), 1.26 (d, J = 6.2 Hz, 6H). ^{13}C NMR (126 MHz, methanol-d_4) δ 155.1, 137.8, 132.8, 130.6, 128.8 (d, J = 31.5 Hz),, 126.7, 126.2, 125.2, 125.1, 111.3, 71.3, 51.4, 17.7. HRMS (ESI†) m/z calcd. for $C_{19}H_{19}F_3N_4O$ $[M + H]^+$ 377.1589, found 377.1590.

(2*S*,6*R*)-2,6-Dimethyl-4-(3-(3-(methylsulfonyl)phenyl) imidazo[1,2-*b*]pyridazin-6-yl)morpholine (8)

Synthesized using substrate **S2**. Pale yellow solid (254 mg, 68%). ^{1}H NMR (500 MHz, methanol-d_4) δ 9.25 (t, J = 1.8 Hz, 1H), 8.23 (ddd, J = 7.9, 1.8, 1.0 Hz, 1H), 8.05 (s, 1H), 7.89 (ddd, J = 7.8, 1.9, 1.1 Hz, 1H), 7.81 (d, J = 10.0 Hz, 1H), 7.71 (t, J = 7.9 Hz, 1H), 7.24 (d, J = 10.0 Hz, 1H), 4.11 (dt, J = 12.1,

 This journal is © The Royal Society of Chemistry 2024

Open Access Article. Published on 28 November 2023. Downloaded on 5/11/2024 5:37:14 AM. This article is licensed under a Creative Commons Attribution-NonCommercial 3.0 Unported Licence.

2.2 Hz, 2H), 3.78 (dqd, J = 10.5, 6.2, 2.4 Hz, 2H), 3.16 (s, 3H), 2.63 (dd, J = 12.9, 10.6 Hz, 2H), 1.29 (d, J = 6.3 Hz, 6H). ^{13}C NMR (126 MHz, methanol-d_4) δ 155.1, 141.2, 137.8, 130.4, 130.4, 130.3, 129.4, 125.9, 125.5, 125.2, 123.9, 110.9, 71.5, 51.2, 43.2, 17.7. HRMS (ESI†) m/z calcd. for $C_{19}H_{22}N_4O_3S$ $[M + H]^+$ 387.1491, found 387.1493.

(2*S*,6*R*)-4-(3-(4-Fluorophenyl) imidazo[1,2-b]pyridazin-6-yl)-2,6-dimethylmorpholine (9)

Synthesized using substrate **S2**. Yellow solid (217 mg, 69%). ^{1}H NMR (500 MHz, methanol-d_4) δ 8.10–8.02 (m, 2H), 7.78 (s, 1H), 7.73 (d, J = 9.9 Hz, 1H), 7.22–7.14 (m, 2H), 7.13 (d, J = 9.9 Hz, 1H), 4.01–3.94 (m, 2H), 3.73 (dqd, J = 10.5, 6.2, 2.4 Hz, 2H), 2.58 (dd, J = 12.9, 10.6 Hz, 2H), 1.23 (d, J = 6.3 Hz, 6H). ^{13}C NMR (126 MHz, DMSO-d_6) δ 161.6 (d, J = 244.9 Hz), 155.0, 137.5, 131.4, 128.4 (d, J = 7.9 Hz), 126.7, 126.5, 126.1, 116.0 (d, J = 21.4 Hz), 110.6, 71.1, 51.5, 19.2. HRMS (ESI†) m/z calcd. for $C_{18}H_{19}FN_4O$ $[M + H]^+$ 327.1621, found 327.1623.

(2*S*,6*R*)-4-(3-(4-Chlorophenyl)imidazo[1,2-*b*]pyridazin-6-yl)-2,6-dimethylmorpholine (10)

Synthesized using substrate **S2**. Yellow solid (246 mg, 74%). ^{1}H NMR (500 MHz, methanol-d_4) δ 8.08–8.01 (m, 2H), 7.83 (s, 1H), 7.74 (d, J = 9.9 Hz, 1H), 7.48–7.40 (m, 2H), 7.15 (d, J = 9.9 Hz, 1H), 3.98 (ddd, J = 12.1, 2.3, 1.0 Hz, 2H), 3.74 (dqd, J = 10.5, 6.2, 2.4 Hz, 2H), 2.59 (dd, J = 12.9, 10.6 Hz, 2H), 1.24 (d, J = 6.3 Hz, 6H). ^{13}C NMR (126 MHz, methanol-d_4) δ 154.9, 137.4, 132.8, 129.6, 128.3, 127.6, 127.5, 127.0, 125.0, 110.7, 71.3, 51.4, 17.7. HRMS (ESI†) m/z calcd. for $C_{18}H_{19}ClN_4O$ $[M + H]^+$ 343.1326, found 343.1331.

(2*S*,6*R*)-2,6-Dimethyl-4-(3-(4-(trifluoromethoxy)phenyl) imidazo[1,2-*b*]pyridazin-6-yl)morpholine (11)

Synthesized using substrate **S2**. Yellow solid (276 mg, 73%). ^{1}H NMR (500 MHz, methanol-d_4) δ 8.22–8.15 (m, 2H), 7.87 (s, 1H), 7.77 (d, J = 10.0 Hz, 1H), 7.37 (ddt, J = 7.9, 2.1, 1.0 Hz, 2H), 7.18 (d, J = 9.9 Hz, 1H), 4.01 (ddd, J = 12.1, 2.3, 1.0 Hz, 2H), 3.76 (dqd, J = 10.4, 6.2, 2.4 Hz, 2H), 2.62 (dd, J = 12.9, 10.6 Hz, 2H), 1.24 (d, J = 6.2 Hz, 6H). ^{13}C NMR (126 MHz, methanol-d_4) δ 155.0, 148.2, 129.8, 128.1, 127.7, 126.9, 125.1, 121.6, 120.7, 119.6, 110.9, 71.3, 51.4, 17.7. HRMS (ESI†) m/z calcd. for $C_{19}H_{19}F_3N_4O_2$ $[M + H]^+$ 393.1538, found 393.1539.

4-(6-((2*S*,6*R*)-2,6-Dimethylmorpholino)imidazo[1,2-*b*] pyridazin-3-yl)benzamide (12)

Synthesized using substrate **S2**. Yellow solid (160 mg, 47%). ^{1}H NMR (500 MHz, methanol-d_4) δ 8.24–8.18 (m, 2H), 8.00–7.92 (m, 3H), 7.77 (d, J = 10.0 Hz, 1H), 7.19 (d, J = 10.0 Hz, 1H), 4.06–3.99 (m, 2H), 3.76 (dqd, J = 12.5, 6.2, 2.3 Hz, 2H), 2.62 (dd, J = 12.9, 10.6 Hz, 2H), 1.25 (d, J = 6.2 Hz, 6H). ^{13}C NMR (126 MHz, methanol-d_4) δ 170.4, 155.0, 137.7, 132.3, 132.0, 130.4, 127.6, 127.2, 125.7, 125.1, 111.1, 71.3, 51.4, 17.7. HRMS (ESI†) m/z calcd. for $C_{19}H_{21}N_5O_2$ $[M + H]^+$ 352.1774, found 352.1777.

4-(6-((2*S*,6*R*)-2,6-dimethylmorpholino)imidazo[1,2-*b*] pyridazin-3-yl)-*N*-methylbenzamide (13)

Synthesized using substrate **S2**. Off-white solid (265 mg, 75%). ^{1}H NMR (500 MHz, methanol-d_4) δ 8.20 (dt, J = 8.4, 2.3 Hz, 2H), 7.95–7.87 (m, 3H), 7.77 (dq, J = 10.1, 2.0 Hz, 1H), 7.19 (dq, J = 10.0, 2.0 Hz, 1H), 4.05–3.99 (m, 2H), 3.81–3.72 (m, 2H), 2.94 (dt, J = 3.1, 1.6 Hz, 3H), 2.62 (ddd, J = 15.1, 11.6, 3.4 Hz, 2H), 1.25 (d, J = 6.3 Hz, 6H).^{13}C NMR (126 MHz, methanol-d_4) δ 168.7, 155.0, 137.7, 132.6, 132.0, 130.4, 127.2, 127.1, 125.7, 125.1, 111.0, 71.3, 51.4, 25.5, 17.7. HRMS (ESI†) m/z calcd. for $C_{20}H_{23}N_5O_2$ $[M+H]^+$ 366.1930, found 366.1933.

2-(4-(6-((2*S*,6*R*)-2,6-Dimethylmorpholino)imidazo[1,2-*b*] pyridazin-3-yl)phenyl)acetonitrile (14)

Synthesized using substrate **S2**. Off-white solid (221 mg, 66%). ^{1}H NMR (500 MHz, methanol-d_4) δ 8.07–8.01 (m, 2H), 7.80 (s, 1H), 7.68 (d, J = 9.9 Hz, 1H), 7.42–7.36 (m, 2H), 7.06 (d, J = 10.0 Hz, 1H), 3.91 (d, J = 14.4 Hz, 4H), 3.69 (dqd, J = 10.6, 6.2, 2.4 Hz, 2H), 2.52 (dd, J = 12.8, 10.6 Hz, 2H), 1.21 (d, J = 6.3 Hz, 6H). ^{13}C NMR (126 MHz, methanol-d_4) δ 153.3, 135.7, 128.5, 128.1, 127.0, 126.3, 125.8, 124.9, 123.4, 116.6, 109.0, 69.7, 49.8, 20.2, 16.2. HRMS (ESI†) m/z calcd. for $C_{20}H_{21}N_5O$ $[M + H]^+$ 348.1824, found 348.1815.

4-(6-((2*S*,6*R*)-2,6-Dimethylmorpholino)imidazo[1,2-*b*] pyridazin-3-yl)benzenesulfonamide (15)

Synthesized using substrate **S2**. Off-white solid (231 mg, 62%). ^{1}H NMR (500 MHz, DMSO-d_6) δ 8.34 (d, J = 8.6 Hz, 2H), 8.12 (s, 1H), 7.96 (d, J = 9.9 Hz, 1H), 7.90 (d, J = 8.6 Hz, 2H), 7.37 (s, 2H), 7.28 (d, J = 10.0 Hz, 1H), 4.08–4.02 (m, 2H), 3.69 (dqd, J = 12.4, 6.1, 2.3 Hz, 2H), 2.57 (dd, J = 12.8, 10.6 Hz, 2H), 1.18 (d, J = 6.2 Hz, 6H). ^{13}C NMR (126 MHz, DMSO-d_6) δ 155.2, 142.5, 138.3, 132.8, 132.7, 126.8, 126.5, 126.1, 126.0, 111.3, 71.2, 51.5, 19.2. HRMS (ESI†) m/z calcd. for $C_{18}H_{21}N_5O_3S$ $[M + H]^+$ 388.1443, found 388.1441.

5-(6-((2*S*,6*R*)-2,6-Dimethylmorpholino)imidazo[1,2-*b*] pyridazin-3-yl)-2-fluorobenzonitrile (16)

Synthesized using substrate **S2**. Pale yellow solid (225 mg, 66%). ^{1}H NMR (500 MHz, Methanol-d_4) δ 8.70 (dd, J = 6.2, 2.3 Hz, 1H), 8.30 (ddd, J = 8.9, 5.0, 2.3 Hz, 1H), 7.95 (s, 1H), 7.79 (d, J = 10.0 Hz, 1H), 7.43 (t, J = 9.0 Hz, 1H), 7.22 (d, J = 10.0 Hz, 1H), 4.01 (ddd, J = 12.1, 2.4, 1.1 Hz, 2H), 3.80 (dqd, J = 10.5, 6.2, 2.4 Hz, 2H), 2.65 (dd, J = 12.9, 10.7 Hz, 2H), 1.29 (d, J = 6.3 Hz, 6H). ^{13}C NMR (126 MHz, methanol-d_4) δ 161.59 (d, J = 258.0 Hz), 155.0, 137.6, 132.7, 132.6, 130.3, 130.1, 126.6, 125.2, 124.9, 116.5 (d, J = 20.2 Hz), 113.4, 111.1, 100.9 (d, J = 15.7 Hz) 71.3, 71.2, 51.3, 17.7. HRMS (ESI†) m/z calcd. for $C_{19}H_{18}FN_5O$ $[M + H]^+$ 352.1574, found 352.1571.

(2*S*,6*R*)-2,6-Dimethyl-4-(3-(pyridin-4-yl)imidazo[1,2-*b*] pyridazin-6-yl)morpholine (17)

Synthesized using substrate **S2**. Off-white solid (176 mg, 59%). ^{1}H NMR (500 MHz, methanol-d_4) δ 8.56–8.51 (m, 2H),

Open Access Article. Published on 28 November 2023. Downloaded on 5/11/2024 5:37:14 AM. This article is licensed under a Creative Commons Attribution-NonCommercial 3.0 Unported Licence.

8.15–8.10 (m, 2H), 8.09 (s, 1H), 7.76 (d, J = 10.0 Hz, 1H), 7.21 (d, J = 10.0 Hz, 1H), 3.99 (ddd, J = 12.1, 2.3, 1.0 Hz, 2H), 3.75 (dqd, J = 10.4, 6.2, 2.4 Hz, 2H), 2.62 (dd, J = 12.8, 10.6 Hz, 2H), 1.26 (d, J = 6.2 Hz, 6H). ^{13}C NMR (126 MHz, methanol-d_4) δ 155.2, 148.9, 138.6, 137.3, 131.9, 125.2, 124.8, 119.7, 111.7, 71.2, 51.3, 17.7. HRMS (ESI) m/z calcd. for $C_{17}H_{19}N_5O$ $[M + H]^+$ 310.1668, found 310.1668.

(2*S*,6*R*)-2,6-Dimethyl-4-(3-(pyridin-3-yl)imidazo[1,2-*b*] pyridazin-6-yl)morpholine (18)

Synthesized using substrate **S2**. Off-white solid (227 mg, 78%). ^{1}H NMR (500 MHz, methanol-d_4) δ 9.28 (d, J = 2.4 Hz, 1H), 8.48–8.39 (m, 2H), 7.92 (d, J = 2.0 Hz, 1H), 7.73 (dd, J = 10.0, 2.0 Hz, 1H), 7.49 (ddd, J = 7.7, 5.0, 2.0 Hz, 1H), 7.15 (dd, J = 10.0, 2.0 Hz, 1H), 3.95 (dd, J = 13.2, 2.5 Hz, 2H), 3.77–3.67 (m, 2H), 2.56 (td, J = 11.7, 2.1 Hz, 2H), 1.23 (d, J = 6.3 Hz, 6H). ^{13}C NMR (126 MHz, methanol-d_4) δ 155.0, 147.1, 145.9, 137.7, 133.8, 130.1, 126.0, 125.1, 124.6, 123.8, 111.2, 71.2, 51.2, 17.7. HRMS (ESI†) m/z calcd. for $C_{17}H_{19}N_5O$ $[M + H]^+$ 310.1668, found 310.1667.

3-(6-((2*S*,6*R*)-2,6-Dimethylmorpholino)imidazo[1,2-*b*] pyridazin-3-yl)benzonitrile (19)

Synthesized using substrate **S2**. Brown solid (224 mg, 70%). ^{1}H NMR (500 MHz, methanol-d_4) δ 8.66–8.61 (m, 1H), 8.23–8.17 (m, 1H), 7.93 (s, 1H), 7.76–7.64 (m, 1H), 7.64–7.51 (m, 2H), 7.15 (dt, J = 10.1, 1.9 Hz, 1H), 4.01–3.93 (m, 2H), 3.75 (dqd, J = 12.5, 6.2, 2.1 Hz, 2H), 2.60 (dd, J = 12.8, 10.5 Hz, 2H), 1.25 (d, J = 6.2 Hz, 6H). ^{13}C NMR (126 MHz, DMSO-d_6) δ 154.8, 138.1, 132.4, 130.7, 130.4, 130.1, 130.0, 128.7, 126.6, 124.9, 119.2, 112.1, 110.9, 71.2, 71.0, 51.4, 19.1. HRMS (ESI†) m/z calcd. for $C_{19}H_{19}N_5O$ $[M + H]^+$ 334.1668, found 334.1667.

(2*S*,6*R*)-4-(3-(1*H*-Indazol-5-yl)imidazo[1,2-*b*]pyridazin-6-yl)-2,6-dimethylmorpholine (20)

Synthesized using substrate **S2**. Pale yellow solid (90 mg, 27%). ^{1}H NMR (500 MHz, methanol-d_4) δ 8.57 (dd, J = 1.6, 0.8 Hz, 1H), 8.06 (d, J = 1.0 Hz, 1H), 7.99 (dd, J = 8.8, 1.6 Hz, 1H), 7.82 (s, 1H), 7.75 (d, J = 9.9 Hz, 1H), 7.61 (dt, J = 8.8, 1.0 Hz, 1H), 7.13 (d, J = 10.0 Hz, 1H), 4.02 (ddd, J = 12.1, 2.3, 1.0 Hz, 2H), 3.75 (dqd, J = 12.5, 6.2, 2.4 Hz, 2H), 2.61 (dd, J = 12.9, 10.6 Hz, 2H), 1.24 (d, J = 6.2 Hz, 6H). ^{13}C NMR (126 MHz, methanol-d_4) δ 154.9, 139.5, 136.9, 134.0, 129.1, 128.6, 126.0, 125.0, 123.0, 121.8, 118.5, 110.3, 109.9, 71.2, 51.5, 17.7. HRMS (ESI†) m/z calcd. for $C_{19}H_{20}N_6O$ $[M+H]^+$ 349.1772, found 349.1785.

(2*S*,6*R*)-4-(3-(1*H*-Indazol-6-yl)imidazo[1,2-*b*]pyridazin-6-yl)-2,6-dimethylmorpholine (21)

Synthesized using substrate **S2**. Pale yellow solid (111 mg, 33%). ^{1}H NMR (500 MHz, DMSO-d_6) δ 8.50 (d, J = 1.5 Hz, 1H), 8.07 (d, J = 2.5 Hz, 2H), 7.95 (d, J = 9.9 Hz, 1H), 7.82 (d, J = 8.5 Hz, 1H), 7.72 (dd, J = 8.5, 1.4 Hz, 1H), 7.26 (d, J = 10.0 Hz, 1H), 4.11–4.04 (m, 2H), 3.71 (dqd, J = 12.4, 6.1, 2.2 Hz, 2H), 2.59 (dd, J = 12.8, 10.6 Hz, 2H), 1.20 (d, J = 6.2 Hz, 7H). ^{13}C NMR (126 MHz, DMSO-d_6) δ 155.1, 140.6, 137.9, 134.0, 132.1, 127.6, 127.1, 126.8, 122.2, 121.1, 119.7, 110.5, 106.9, 71.2, 51.6, 19.3. HRMS (ESI†) m/z calcd. for $C_{19}H_{20}N_6O$ $[M + H]^+$ 349.1772, found 349.1783.

(2*S*,6*R*)-4-(3-(1*H*-Indazol-4-yl)imidazo[1,2-*b*]pyridazin-6-yl)-2,6-dimethylmorpholine (22)

Synthesized using substrate **S2**. Yellow solid (141 mg, 42%). ^{1}H NMR (500 MHz, methanol-d_4) δ 8.17 (s, 1H), 7.90 (s, 1H), 7.81–7.75 (m, 2H), 7.57 (d, J = 8.4 Hz, 1H), 7.47 (dd, J = 8.5, 7.1 Hz, 1H), 7.15 (d, J = 10.0 Hz, 1H), 3.96–3.89 (m, 2H), 3.67 (dqd, J = 12.4, 6.2, 2.2 Hz, 2H), 2.51 (dd, J = 12.9, 10.6 Hz, 2H), 1.16 (d, J = 6.2 Hz, 6H). ^{13}C NMR (126 MHz, methanol-d_4) δ 154.7, 140.6, 137.2, 133.9, 130.8, 127.2, 126.4, 125.0, 121.4, 120.5, 120.0, 110.9, 109.6, 71.3, 51.2, 17.6. HRMS (ESI†) m/z calcd. for $C_{19}H_{20}N_6O$ $[M + H]^+$ 349.1772, found 349.1783.

(2*S*,6*R*)-2,6-Dimethyl-4-(3-(1-methyl-1*H*-indazol-6-yl) imidazo[1,2-*b*]pyridazin-6-yl)morpholine (23)

Synthesized using substrate **S2**. Off-white solid (313 mg, 90%). ^{1}H NMR (500 MHz, methanol-d_4) δ 8.57 (s, 1H), 7.98 (s, 1H), 7.96 (s, 1H), 7.77–7.71 (m, 2H), 7.68 (d, J = 8.6 Hz, 1H), 7.14 (dt, J = 10.0, 1.7 Hz, 1H), 4.03–3.95 (m, 5H), 3.77 (dtt, J = 12.4, 6.1, 3.6 Hz, 2H), 2.59 (t, J = 11.5 Hz, 2H), 1.24 (d, J = 6.2 Hz, 6H). ^{13}C NMR (126 MHz, methanol-d_4) δ 154.9, 139.8, 137.5, 132.2, 130.1, 127.4, 127.1, 124.8, 122.4, 120.7, 119.0, 110.3, 105.4, 71.2, 51.3, 34.1, 17.8. HRMS (ESI†) m/z calcd. for $C_{20}H_{22}N_6O$ $[M + H]^+$ 363.1928, found 363.1932.

(2*S*,6*R*)-2,6-Dimethyl-4-(3-(1-methyl-1*H*-indazol-5-yl) imidazo[1,2-*b*]pyridazin-6-yl)morpholine (24)

Synthesized using substrate **S2**. Off-white solid (334 mg, 96%). ^{1}H NMR (500 MHz, methanol-d_4) δ 8.50 (dd, J = 1.6, 0.8 Hz, 1H), 8.01–7.95 (m, 2H), 7.80 (s, 1H), 7.72 (d, J = 9.9 Hz, 1H), 7.57 (dt, J = 8.9, 0.9 Hz, 1H), 7.09 (d, J = 9.9 Hz, 1H), 4.07 (s, 3H), 3.97 (ddd, J = 12.0, 2.3, 1.0 Hz, 2H), 3.71 (ddt, J = 12.5, 6.2, 3.1 Hz, 2H), 2.56 (dd, J = 12.8, 10.6 Hz, 2H), 1.22 (d, J = 6.2 Hz, 6H). ^{13}C NMR (126 MHz, methanol-d_4) δ 154.8, 139.1, 136.9, 132.8, 129.1, 128.3, 125.7, 124.9, 123.8, 121.7, 118.5, 110.2, 109.0, 71.2, 51.4, 34.3, 17.7. HRMS (ESI†) m/z calcd. for $C_{20}H_{22}N_6O$ $[M + H]^+$ 363.1928, found 363.1934.

(2*S*,6*R*)-4-(3-(3-Ethyl-1*H*-indazol-5-yl)imidazo[1,2-*b*]pyridazin-6-yl)-2,6-dimethylmorpholine (25)

Synthesized using substrate **S2**. Off-white solid (49 mg, 25%). ^{1}H NMR (500 MHz, DMSO-d_6) δ 8.85 (dd, J = 1.6, 0.8 Hz, 1H), 8.02 (s, 1H), 7.96–7.87 (m, 2H), 7.56–7.50 (m, 1H), 7.22 (d, J = 9.9 Hz, 1H), 4.10–4.03 (m, 2H), 3.72 (dqd, J = 12.3, 6.0, 2.2 Hz, 2H), 2.96 (q, J = 7.6 Hz, 2H), 2.58 (dd, J = 12.6, 10.5 Hz, 2H), 1.34 (t, J = 7.6 Hz, 3H), 1.18 (d, J = 6.2 Hz, 6H). ^{13}C NMR (126 MHz, DMSO-d_6) δ 155.2, 147.5, 140.4, 137.5, 131.0, 127.9, 126.6, 125.4, 121.8, 121.1, 116.9, 111.0, 110.1, 71.2,

 This journal is © The Royal Society of Chemistry 2024

Open Access Article. Published on 28 November 2023. Downloaded on 5/11/2024 5:37:14 AM. This article is licensed under a Creative Commons Attribution-NonCommercial 3.0 Unported Licence.

51.7, 20.3, 19.2, 14.1. HRMS (ESI†) *m*/*z* calcd. for $C_{21}H_{14}N_6O$ $[M + H]^+$ 377.2089, found 377.2089.

(2*S*,6*R*)-4-(3-(3-Cyclopropyl-1*H*-indazol-5-yl)imidazo[1,2-*b*] pyridazin-6-yl)-2,6-dimethylmorpholine (26)

Synthesized using substrate **S2**. Pale yellow solid (50 mg, 30%). ^{1}H NMR (500 MHz, DMSO-d_6) δ 8.83 (d, J = 1.2 Hz, 1H), 8.00 (s, 1H), 7.96–7.86 (m, 2H), 7.54–7.49 (m, 1H), 7.22 (d, J = 10.0 Hz, 1H), 4.10–4.04 (m, 2H), 3.71 (dqd, J = 12.3, 6.1, 2.2 Hz, 2H), 2.58 (dd, J = 12.7, 10.6 Hz, 2H), 2.27 (tt, J = 7.6, 6.1 Hz, 1H), 1.16 (d, J = 6.2 Hz, 6H), 1.03–0.96 (m, 4H). ^{13}C NMR (126 MHz, DMSO-d_6) δ 155.2, 147.3, 140.5, 137.5, 131.0, 127.9, 126.6, 125.6, 122.0, 121.1, 116.9, 111.0, 110.1, 71.2, 51.7, 19.2, 8.5, 7.9. HRMS (ESI†) *m*/*z* calcd. for $C_{22}H_{24}N_6O$ $[M + H]^+$ 389.2089, found 389.2086.

5-(6-((2*S*,6*R*)-2,6-Dimethylmorpholino)imidazo[1,2-*b*] pyridazin-3-yl)indolin-2-one (27)

Synthesized using substrate **S2**. Off-white solid (76 mg, 45%). ^{1}H NMR (500 MHz, methanol-d_4) δ 7.95–7.88 (m, 2H), 7.75–7.68 (m, 2H), 7.09 (d, J = 10.0 Hz, 1H), 6.93 (d, J = 8.1 Hz, 1H), 4.00–3.94 (m, 2H), 3.74 (dqd, J = 12.4, 6.1, 2.3 Hz, 2H), 3.54 (s, 2H), 2.58 (dd, J = 12.8, 10.6 Hz, 2H), 1.23 (d, J = 6.2 Hz, 6H). ^{13}C NMR (126 MHz, methanol-d_4) δ 178.4, 154.8, 142.7, 136.9, 128.7, 128.2, 126.0, 126.0, 124.9, 123.1, 122.6, 110.1, 109.2, 71.2, 51.5, 35.7, 17.7. HRMS (ESI†) *m*/*z* calcd. for $C_{20}H_{21}N_5O_2$ $[M + H]^+$ 364.1774, found 364.1771.

(2*S*,6*R*)-4-(3-Bromo-2-methylimidazo[1,2-*b*]pyridazin-6-yl)-2,6-dimethylmorpholine (S4)

Pale yellow solid (425 mg, 82%). ^{1}H NMR (500 MHz, methanol-d_4) δ 7.56 (d, J = 9.8 Hz, 1H), 7.04 (d, J = 9.9 Hz, 1H), 4.00 (ddd, J = 12.1, 2.4, 1.1 Hz, 2H), 3.70 (dqd, J = 10.5, 6.2, 2.4 Hz, 2H), 2.51 (dd, J = 12.9, 10.6 Hz, 2H), 2.33 (s, 3H), 1.22 (d, J = 6.3 Hz, 6H). ^{13}C NMR (126 MHz, methanol-d_4) δ 154.9, 139.1, 136.0, 124.0, 110.2, 98.3, 71.3, 51.0, 17.7, 12.2. HRMS (ESI†) *m*/*z* calcd. for $C_{13}H_{17}BrN_4O$ $[M + H]^+$ 325.2189, found 325.2186.

(2*S*,6*R*)-2,6-Dimethyl-4-(2-methyl-3-(3-methyl-1*H*-indazol-5-yl) imidazo[1,2-*b*]pyridazin-6-yl)morpholine (28)

Synthesized using substrate **S4**. Yellow solid (242 mg, 67%). ^{1}H NMR (500 MHz, methanol-d_4) δ 8.04 (dd, J = 1.6, 0.9 Hz, 1H), 7.67–7.57 (m, 2H), 7.51 (dd, J = 8.7, 0.9 Hz, 1H), 6.99 (d, J = 9.9 Hz, 1H), 3.89–3.81 (m, 2H), 3.63 (dqd, J = 12.3, 6.1, 2.2 Hz, 2H), 2.52 (s, 3H), 2.50–2.38 (m, 5H), 1.13 (d, J = 6.2 Hz, 6H). ^{13}C NMR (126 MHz, methanol-d_4) δ 154.4, 142.3, 140.3, 138.1, 134.8, 127.9, 125.0, 123.9, 122.0, 120.7, 120.5, 109.8, 109.4, 71.3, 71.2, 51.3, 51.2, 17.7, 13.4, 10.3. HRMS (ESI†) *m*/*z* calcd. for $C_{21}H_{24}N_6O$ $[M + H]^+$ 377.2089, found 377.2087.

(1*R*,4*R*)-5-(3-Bromoimidazo[1,2-*b*]pyridazin-6-yl)-2-oxa-5-azabicyclo[2.2.1]heptane (S5)

Off-white solid (478 mg, 75%). ^{1}H NMR (500 MHz, methanol-d_4) δ 7.66 (d, J = 9.8 Hz, 1H), 7.45 (s, 1H), 6.86 (d, J = 9.8 Hz, 1H), 4.90–4.86 (m, 1H), 4.73–4.69 (m, 1H), 3.88 (s, 2H), 3.59 (dd, J = 10.0, 1.6 Hz, 1H), 3.48–3.42 (m, 1H), 2.06–1.96 (m, 2H); ^{13}C NMR (126 MHz, methanol-d_4) δ 153.3, 136.7, 130.3, 124.8, 111.0, 99.7, 76.2, 72.7, 57.2, 56.2, 35.9. HRMS (ESI†) *m*/*z* calcd. for $C_{11}H_{12}BrN_4O$ $[M + H]^+$ 295.0194, found 295.0193.

(1*R*,4*R*)-5-(3-(3-Methyl-1*H*-indazol-5-yl)imidazo[1,2-*b*] pyridazin-6-yl)-2-oxa-5-azabicyclo[2.2.1]heptane (29)

Synthesized using substrate **S5**. Off-white solid (51 mg, 64%). ^{1}H NMR (500 MHz, methanol-d_4) δ 8.66 (s, 1H), 7.96 (dd, J = 8.8, 1.6 Hz, 1H), 7.84 (s, 1H), 7.75 (d, J = 9.8 Hz, 1H), 7.52 (d, J = 8.8 Hz, 1H), 6.88 (d, J = 9.8 Hz, 1H), 4.74 (d, J = 2.4 Hz, 1H), 3.98 (d, J = 7.6 Hz, 1H), 3.92 (dd, J = 7.6, 1.5 Hz, 1H), 3.66 (dd, J = 9.8, 1.5 Hz, 1H), 3.50 (d, J = 9.8 Hz, 1H), 2.57 (s, 3H), 2.11–1.94 (m, 2H), 1.27 (s, 1H). ^{13}C NMR (126 MHz, methanol-d_4) δ 152.8, 142.6, 128.6, 125.8, 125.0, 122.1, 121.2, 117.6, 110.1, 109.9, 76.3, 72.6, 57.5, 56.5, 47.1, 36.1, 10.3. HRMS (ESI†) *m*/*z* calcd. for $C_{19}H_{18}N_6O$ $[M + H]^+$ 347.1620, found 347.1624.

(1*S*,4*S*)-5-(3-Bromoimidazo[1,2-*b*]pyridazin-6-yl)-2-oxa-5-azabicyclo[2.2.1]heptane (S6)

Off-white solid (506 mg, 79%). ^{1}H NMR (500 MHz, methanol-d_4) δ 7.71–7.63 (m, 1H), 7.48–7.43 (m, 1H), 6.91–6.84 (m, 1H), 4.89 (d, J = 5.3 Hz, 2H), 4.72 (s, 1H), 3.91–3.86 (m, 2H), 3.63–3.56 (m, 1H), 3.49–3.43 (m, 1H), 2.07–1.95 (m, 2H); ^{13}C NMR (126 MHz, methanol-d_4) δ 153.3, 136.7, 130.3, 124.8, 111.0, 99.8, 76.2, 72.7, 57.3, 56.2, 35.9. HRMS (ESI†) *m*/*z* calcd. for $C_{11}H_{12}BrN_4O$ $[M + H]^+$ 295.0194, found 295.0193.

(1*S*,4*S*)-5-(3-(3-Methyl-1*H*-indazol-5-yl)imidazo[1,2-*b*]pyridazin-6-yl)-2-oxa-5-azabicyclo[2.2.1]heptane (30)

Synthesized using substrate **S6**. Off-white solid (65 mg, 93%). ^{1}H NMR (500 MHz, methanol-d_4) δ 8.69 (t, J = 1.1 Hz, 1H), 8.00 (dd, J = 8.8, 1.5 Hz, 1H), 7.90–7.69 (m, 2H), 7.54 (d, J = 8.8 Hz, 1H), 6.92 (d, J = 9.7 Hz, 1H), 4.00 (d, J = 7.6 Hz, 1H), 3.94 (dd, J = 7.6, 1.5 Hz, 1H), 3.69 (dd, J = 9.9, 1.5 Hz, 1H), 3.52 (d, J = 9.7 Hz, 1H), 2.59 (s, 3H), 2.13–2.01 (m, 2H), 1.28 (s, 1H). ^{13}C NMR (126 MHz, methanol-d_4) δ 152.8, 142.6, 140.4, 131.5, 126.4, 125.8, 125.0, 122.1, 121.2, 117.6, 110.1, 109.9, 108.8, 76.3, 72.6, 57.5, 56.5, 36.1, 10.3, 10.2. HRMS (ESI†) *m*/*z* calcd. for $C_{19}H_{18}N_6O$ $[M + H]^+$ 347.1620, found 347.1625.

4-(3-Bromoimidazo[1,2-*b*]pyridazin-6-yl)-2,2-dimethylmorpholine (S7)

Off-white solid (571 mg, 85%). ^{1}H NMR (500 MHz, DMSO-d_6) δ 7.86 (d, J = 10.0 Hz, 1H), 7.58 (s, 1H), 7.21 (d, J = 9.9 Hz, 1H), 3.77–3.67 (m, 2H), 3.48 (dd, J = 6.2, 4.0 Hz, 2H), 1.19 (s, 6H); ^{13}C NMR (126 MHz, chloroform-d) δ 155.3, 136.9, 132.2,

Open Access Article. Published on 28 November 2023. Downloaded on 5/11/2024 5:37:14 AM. This article is licensed under a Creative Commons Attribution-NonCommercial 3.0 Unported Licence.

126.1, 109.4, 100.3, 71.3, 60.4, 55.4, 45.7, 24.6. HRMS (ESI†) *m*/*z* calcd. for $C_{12}H_{16}BrN_4O$ $[M + H]^+$ 311.0507, found 311.0506.

2,2-Dimethyl-4-(3-(3-methyl-1*H*-indazol-5-yl)imidazo[1,2-*b*]pyridazin-6-yl)morpholine (31)

Synthesized using substrate **S7**. Yellow solid (178 mg, 51%). ^{1}H NMR (500 MHz, methanol-d_4) δ 8.68 (s, 1H), 7.95 (dt, J = 8.9, 1.8 Hz, 1H), 7.87 (d, J = 2.4 Hz, 1H), 7.79 (dd, J = 9.9, 2.3 Hz, 1H), 7.54 (dd, J = 8.8, 2.4 Hz, 1H), 7.15 (dd, J = 9.9, 2.4 Hz, 1H), 3.90 (q, J = 3.9 Hz, 2H), 3.57 (dt, J = 6.9, 3.0 Hz, 2H), 3.45 (d, J = 2.4 Hz, 2H), 2.59 (d, J = 2.5 Hz, 3H), 1.32 (d, J = 2.4 Hz, 6H). ^{13}C NMR (126 MHz, DMSO-d_6) δ 155.4, 142.1, 140.2, 137.3, 130.9, 127.8, 126.6, 125.3, 122.7, 121.1, 117.2, 110.8, 109.9, 71.2, 60.1, 55.3, 46.2, 24.9, 12.1. HRMS (ESI†) *m*/*z* calcd. for $C_{20}H_{22}N_6O$ $[M + H]^+$ 363.1933, found 363.1931.

(*R*)-4-(3-Bromoimidazo[1,2-*b*]pyridazin-6-yl)-2-methylmorpholine (S8)

Off-white solid (501 mg, 78%). ^{1}H NMR (500 MHz, DMSO-d_6) δ 7.87 (d, J = 9.9 Hz, 1H), 7.59 (s, 1H), 7.22 (d, J = 10.0 Hz, 1H), 4.14–3.84 (m, 3H), 3.71–3.51 (m, 2H), 2.92 (ddd, J = 12.9, 11.9, 3.5 Hz, 1H), 2.70–2.54 (m, 1H), 1.15 (d, J = 6.2 Hz, 3H); ^{13}C NMR (126 MHz, DMSO-d_6) δ 155.6, 137.1, 132.0, 126.5, 111.0, 99.8, 71.3, 65.8, 51.8, 45.4, 19.1. HRMS (ESI†) *m*/*z* calcd. for $C_{11}H_{14}BrN_4O$ $[M + H]^+$ 297.0351, found 297.0348.

(*R*)-2-Methyl-4-(3-(3-methyl-1*H*-indazol-5-yl)imidazo[1,2-*b*]pyridazin-6-yl)morpholine (32)

Synthesized using substrate **S8**. Off-white solid (151 mg, 42%). ^{1}H NMR (500 MHz, DMSO-d_6) δ 8.77 (dd, J = 1.6, 0.8 Hz, 1H), 8.02 (s, 1H), 7.98–7.87 (m, 2H), 7.52 (dd, J = 8.7, 0.8 Hz, 1H), 7.20 (d, J = 10.0 Hz, 1H), 4.07 (dt, J = 12.5, 2.1 Hz, 1H), 4.03–3.92 (m, 2H), 3.71–3.61 (m, 2H), 3.02–2.93 (m, 1H), 2.67 (dd, J = 12.7, 10.4 Hz, 1H), 2.51 (s, 3H), 1.18 (d, J = 6.2 Hz, 3H). ^{13}C NMR (126 MHz, DMSO-d_6) δ 155.2, 142.1, 140.2, 137.4, 130.9, 127.9, 126.6, 125.3, 122.7, 121.1, 117.2, 110.8, 109.9, 71.2, 66.0, 52.3, 46.1, 19.3, 12.0. HRMS (ESI†) *m*/*z* calcd. for $C_{19}H_{20}N_6O$ $[M + H]^+$ 349.1777, found 349.1779.

(*S*)-4-(3-Bromoimidazo[1,2-*b*]pyridazin-6-yl)-2-methylmorpholine (S9)

Off-white solid (449 mg, 69%). ^{1}H NMR (500 MHz, methanol-d_4) δ 7.71 (d, J = 10.0 Hz, 1H), 7.50 (s, 1H), 7.17 (d, J = 10.0 Hz, 1H), 4.12–3.96 (m, 3H), 3.76–3.65 (m, 2H), 3.02 (ddd, J = 13.0, 11.9, 3.5 Hz, 1H), 2.69 (dd, J = 12.9, 10.4 Hz, 1H), 1.24 (d, J = 6.3 Hz, 3H); ^{13}C NMR (126 MHz, methanol-d_4) δ 155.5, 136.9, 130.7, 124.9, 110.8, 100.2, 71.4, 65.8, 51.6, 45.1, 17.6. HRMS (ESI†) *m*/*z* calcd. for $C_{11}H_{14}BrN_4O$ $[M + H]^+$ 297.0351, found 297.0348.

(*S*)-2-Methyl-4-(3-(3-methyl-1*H*-indazol-5-yl)imidazo[1,2-*b*]pyridazin-6-yl)morpholine (33)

Synthesized using substrate **S9**. Off-white solid (146 mg, 41%). ^{1}H NMR (500 MHz, DMSO-d_6) δ 8.79–8.75 (m, 1H), 8.01 (s, 1H), 7.97–7.89 (m, 2H), 7.52 (dd, J = 8.8, 0.8 Hz, 1H), 7.19 (d, J = 9.9 Hz, 1H), 4.06 (dt, J = 12.5, 2.1 Hz, 1H), 3.96 (dddd, J = 12.9, 8.4, 3.1, 1.3 Hz, 2H), 3.71–3.61 (m, 2H), 3.02–2.92 (m, 1H), 2.66 (dd, J = 12.7, 10.4 Hz, 1H), 2.51 (s, 3H), 1.18 (d, J = 6.2 Hz, 3H). ^{13}C NMR (126 MHz, DMSO-d_6) δ 155.2, 142.1, 140.2, 137.4, 130.9, 127.9, 126.6, 125.3, 122.7, 121.1, 117.2, 110.8, 109.9, 71.2, 66.0, 52.3, 46.1, 19.3, 12.0. HRMS (ESI†) *m*/*z* calcd. for $C_{19}H_{20}N_6O$ $[M+H]^+$ 349.1779, found 349.1774.

3-(3-Bromoimidazo[1,2-*b*]pyridazin-6-yl)-8-oxa-3-azabicyclo[3.2.1]octane (S10)

Off-white solid (514 mg, 77%). ^{1}H NMR (500 MHz, DMSO-d_6) δ 7.85 (d, J = 10.0 Hz, 1H), 7.58 (s, 1H), 7.13 (d, J = 10.0 Hz, 1H), 4.57–4.37 (m, 2H), 3.78 (d, J = 12.3 Hz, 2H), 3.06 (dd, J = 12.6, 2.6 Hz, 2H), 1.95–1.67 (m, 4H); ^{13}C NMR (126 MHz, DMSO-d_6) δ 156.3, 137.1, 131.9, 126.3, 110.4, 99.6, 73.1, 51.3, 28.0. HRMS (ESI†) *m*/*z* calcd. for $C_{12}H_{14}BrN_4O$ $[M + H]^+$ 309.0351, found 309.0349.

3-(3-(3-Methyl-1*H*-indazol-5-yl)imidazo[1,2-*b*]pyridazin-6-yl)-8-oxa-3-azabicyclo[3.2.1]octane (34)

Synthesized using substrate **S10**. Off-white solid (39 mg, 19%). ^{1}H NMR (500 MHz, methanol-d_4) δ 8.65 (dd, J = 1.6, 0.8 Hz, 1H), 7.99 (dd, J = 8.8, 1.6 Hz, 1H), 7.87 (s, 1H), 7.79 (d, J = 9.9 Hz, 1H), 7.54 (dd, J = 8.8, 0.9 Hz, 1H), 7.11 (d, J = 10.0 Hz, 1H), 4.53 (dd, J = 4.5, 2.4 Hz, 2H), 3.85 (dt, J = 12.6, 1.1 Hz, 2H), 3.24 (dd, J = 12.4, 2.6 Hz, 2H), 2.59 (s, 3H), 2.03–1.88 (m, 4H). ^{13}C NMR (126 MHz, methanol-d_4) δ 155.7, 142.7, 140.3, 137.0, 128.9, 128.5, 125.9, 124.9, 122.1, 121.1, 117.8, 109.9, 109.3, 73.8, 51.3, 27.6, 10.3. HRMS (ESI†) *m*/*z* calcd. for $C_{20}H_{20}N_6O$ $[M + H]^+$ 361.1777, found 361.1763.

(2*S*,6*S*)-4-(3-Bromoimidazo[1,2-*b*]pyridazin-6-yl)-2,6-dimethylmorpholine (S11)

Off-white solid (236 mg, 35%). ^{1}H NMR (500 MHz, chloroform-*d*) δ 7.68 (d, J = 9.9 Hz, 1H), 7.53 (s, 1H), 6.79 (d, J = 9.9 Hz, 1H), 4.27–4.06 (m, 2H), 3.65 (dd, J = 12.8, 3.4 Hz, 2H), 3.27 (dd, J = 12.8, 6.3 Hz, 2H), 1.30 (d, J = 6.4 Hz, 6H); ^{13}C NMR (125 MHz, chloroform-*d*) δ 155.4, 136.8, 132.0, 126.0, 109.4, 100.3, 66.0, 50.7, 17.9. HRMS (ESI†) *m*/*z* calcd. for $C_{12}H_{16}BrN_4O$ $[M + H]^+$ 311.0507, found 311.0507.

(2*R*,6*R*)-2,6-Dimethyl-4-(3-(3-methyl-1*H*-indazol-5-yl)imidazo[1,2-b]pyridazin-6-yl)morpholine (35)

Synthesized using substrate **S11**. Brown solid (131 mg, 37%). ^{1}H NMR (500 MHz, methanol-d_4) δ 8.66 (s, 1H), 7.90 (d, J = 8.8 Hz, 1H), 7.84 (s, 1H), 7.72 (d, J = 9.8 Hz, 1H), 7.49 (d, J = 8.7 Hz, 1H), 7.07 (d, J = 9.8 Hz, 1H), 4.15 (tt, J = 6.4, 3.4 Hz, 2H), 3.62 (dd, J = 12.8, 3.4 Hz, 2H), 3.26 (dd, J = 12.7, 6.4 Hz, 2H), 2.54 (d, J = 5.5 Hz, 3H), 1.27 (d, J = 6.4 Hz, 6H). ^{13}C NMR

This journal is © The Royal Society of Chemistry 2024

Open Access Article. Published on 28 November 2023. Downloaded on 5/11/2024 5:37:14 AM. This article is licensed under a Creative Commons Attribution-NonCommercial 3.0 Unported Licence.

(126 MHz, methanol-d_4) δ 155.2, 142.5, 140.2, 136.9, 128.8, 128.2, 125.5, 124.8, 122.0, 121.0, 117.2, 109.9, 109.7, 66.0, 50.6, 16.8, 10.4. HRMS (ESI†) *m*/*z* calcd. for $C_{20}H_{22}N_6O$ $[M + H]^+$ 363.1933, found 363.1931.

Cell viability assays

The myeloma cell lines used in this study were MPC-11 and H929. MPC-11 cells were maintained in DMEM with 10% FBS and H292 cells were maintained in RPMI with 10% heat-inactivated FBS. All cells were purchased from ATCC and maintained in culture below 10 passages. All cells were cultured at 37 °C in a humidified atmosphere containing 5% CO_2. 4–5 × 10^3 cells were seeded in 96 well plates and incubated for 24 hours. Cells were then treated with various concentrations of indicated compounds for 72 hours. After the indicated period of treatment, the CellTiter-Blue cell viability assay reagent (Promega) was added based on the manufacturer's recommendations and incubated for 3 hours. The fluorescence ($\lambda_{ex/em}$ = 560/590 nm) of each well was quantified *via* a Biotek Cytation 5 multi-mode reader. Experiments were performed in triplicate, with data reported as the mean and standard deviation of 3 data points. Readings from treated groups were normalized to cells treated with DMSO.

Evaluation of pTAK1 levels in MPC-11 cells *via* western blot

0.5–1 × 10^6 MPC-11 cells were seeded in 6-well plates. After 24 h, the cells were treated with compounds **26**, **3**, and takinib for 48 h. The cells were then lysed with RIPA lysis buffer (50 mM Tris (pH 7.4), 150 mM NaCl, 1% Triton X-100, 0.1% sodium dodecyl sulfate (SDS), 0.5% sodium deoxycholate) with protease inhibitor cocktail (Roche) and 1 mM phenylmethylsulfonyl fluoride (Themo-Fisher Scientific). The cells were centrifuged and the supernatant was collected into new 1.5 mL Eppendorf tubes. The Pierce Rapid Gold BCA Protein Assay Kit (Thermo-Fisher) was used to quantify total protein. Next, the proteins were separated using 10% SDS polyacrylamide gel electrophoresis and transferred to a polyvinylidene difluoride (PVDF) membrane. The membrane was probed with pTAK1 (CST #9339), TAK1 (CST, #4505), and β-actin (CST #8457) antibodies overnight at 4 °C. After overnight incubation, the membrane was washed and further incubated with the corresponding horseradish peroxidase (HRP)-conjugated secondary antibodies at 24 °C for 2 h. A SuperSignal West Pico PLUS chemiluminescent substrate (Thermo-Fisher) was used for signal detection on an Azure 300 imaging system (Azure Biosystems). All antibodies were purchased from Cell Signaling Technology.

Author contributions

HOS designed and supervised the project. DA and ND synthesized the compounds. DA performed the kinase assays. ALK and JL performed cell culture. NRB performed computational docking. All authors were involved in the writing of the manuscript.

Conflicts of interest

HOS is a co-founder of KinaRx Inc., a company developing kinase inhibitors for potential oncology applications.

Acknowledgements

We thank The Paula and Rodger Riney Foundation and the Purdue Institute for Cancer Research for funding.

References

1 S. V. Rajkumar, *Am. J. Hematol.*, 2020, **95**, 548–567.
2 A. Palumbo, K. Anderson and S. G. Battista, *Clin. Cancer Res.*, 2016, **22**, 5419–5427.
3 K. L. Wu and P. Sonneveld, *Clin. Lymphoma Myeloma*, 2005, **6**, 96–101.
4 D. E. Reece, *Hematology Am. Soc. Hematol. Educ. Program*, 2005, **1**, 353–359.
5 M. S. Raab, K. Podar, I. Breitkreutz, P. G. Richardson and K. C. Anderson, *Int. J. Mol. Sci.*, 2022, **23**, 1649.
6 S. V. Rajkumar and R. A. Kyle, *Mayo Clin. Proc.*, 2005, **80**, 1371–1382.
7 N. Giuliani, V. Rizzoli and G. D. Roodman, *Blood*, 2006, **108**, 3992–3996.
8 T. Hideshima, P. Richardson, D. Chauhan, V. J. Palombella, P. J. Elliott, J. Adams and K. C. Anderson, *Cancer Res.*, 2001, **61**, 3071–3076.
9 S. Aashaq, A. Batool and K. I. Andrabi, *Apoptosis*, 2019, **24**, 3–20.
10 M. Nishimura, M.-S. Shin, P. Singhirunnusorn, S. Suzuki, M. Kawanishi, K. Koizumi, I. Saiki and H. Sakurai, *Mol. Cell. Biol.*, 2009, **29**, 5529–5539.
11 B. Skaug, X. Jiang and Z. J. Chen, *Annu. Rev. Biochem.*, 2009, **78**, 769–796.
12 A. A. Ajibade, H. Y. Wang and R. F. Wang, *Trends Immunol.*, 2013, **34**, 307–316.
13 A. Adhikari, M. Xu and Z. J. Chen, *Oncogene*, 2007, **26**, 3214–3226.
14 H. Sakurai, *Trends Pharmacol. Sci.*, 2012, **33**, 522–530.
15 J. Li, C. Liang, Z. K. Zhang, X. Pan, S. Peng, W. S. Lee, A. Lu, Z. Lin, G. Zhang, W. N. Leung and B. T. Zhang, *Cell Discovery*, 2017, **3**, 17023.
16 R. Niesvizky, D. Siegel and J. Michaeli, *Med. J. Aust.*, 2019, **210**, 375–380.
17 K. J. Gordon and G. C. Blobe, *Biochim. Biophys. Acta*, 2008, **1782**, 197–228.
18 D. E. Joshua, C. Bryant, C. Dix, J. Gibson and J. Ho, *Med. J. Aust.*, 2019, **210**, 375–380.
19 K. Podar, G. Tonon, M. Sattler, Y.-T. Tai, S. Legouill, H. Yasui, K. Ishitsuka, S. Kumar, R. Kumar, L. N. Pandite, T. Hideshima, D. Chauhan and K. C. Anderson, *Proc. Natl. Acad. Sci. U. S. A.*, 2006, **103**, 19478–19483.

Open Access Article. Published on 28 November 2023. Downloaded on 5/11/2024 5:37:14 AM.
This article is licensed under a Creative Commons Attribution-NonCommercial 3.0 Unported Licence.

20 J. Teramachi, H. Tenshin, M. Hiasa, A. Oda, A. Bat-Erdene, T. Harada, S. Nakamura, M. Ashtar, S. Shimizu, M. Iwasa, K. Sogabe, M. Oura, S. Fujii, K. Kagawa, H. Miki, I. Endo, T. Haneji, T. Matsumoto and M. Abe, *Haematologica*, 2021, **106**, 1401–1413.
21 T. Harada, M. Hiasa, J. Teramachi and M. Abe, *Cancers*, 2021, **13**, 4441.
22 J. Totzke, D. Gurbani, R. Raphemot, P. F. Hughes, K. Bodoor, D. A. Carlson, D. R. Loiselle, A. K. Bera, L. S. Eibschutz, M. M. Perkins, A. L. Eubanks, P. L. Campbell, D. A. Fox, K. D. Westover, T. A. J. Haystead and E. R. Derbyshire, *Cell Chem. Biol.*, 2017, **24**, 1029–1039.
23 A. Fauster, M. Rebsamen, K. V. M. Huber, J. W. Bigenzahn, A. Stukalov, C. H. Lardeau, S. Scorzoni, M. Bruckner, M. Gridling, K. Parapatics, J. Colinge, K. L. Bennett, S. Kubicek, S. Krautwald, A. Linkermann and G. Superti-Furga, *Cell Death Dis.*, 2015, **6**, e1767.
24 A. Garrido, G. Vera, P. O. Delaye and C. Enguehard-Gueiffier, *Eur. J. Med. Chem.*, 2021, **226**, 113867.
25 M. Al-Ghorbani, B. A. Begum, M. S. Zabiulla and S. Ara Khanum, *J. Chem. Pharm. Res.*, 2015, **7**, 281–301.
26 E. Vitaku, D. T. Smith and J. T. Njardarson, *J. Med. Chem.*, 2014, **57**, 10257–10274.
27 H. Zegzouti, M. Zdanovskaia, K. Hsiao and S. A. Goueli, *Assay Drug Dev. Technol.*, 2009, **7**, 560–572.
28 C. A. Lipinski, *Drug Discovery Today: Technol.*, 2004, **1**, 337–341.
29 L. M. Lima and E. J. Barreiro, *Curr. Med. Chem.*, 2005, **12**, 23–49.
30 A. Gomtsyan, *Chem. Heterocycl. Compd.*, 2012, **48**, 7–10.
31 X. Chen, S. Hussain, S. Parveen, S. Zhang, Y. Yang and C. Zhu, *Curr. Med. Chem.*, 2012, **19**, 3578–3604.
32 A. Ovung and J. Bhattacharyya, *Biophys. Rev.*, 2021, **13**, 259–272.
33 E. Lenci, L. Calugi and A. Trabocchi, *ACS Chem. Neurosci.*, 2021, **12**, 378–390.
34 A. Kumari and R. K. Singh, *Bioorg. Chem.*, 2020, **96**, 103578.
35 A. P. Kourounakis, D. Xanthopoulos and A. Tzara, *Med. Res. Rev.*, 2020, **40**, 709–752.
36 C. Ouyang, L. Nie, M. Gu, A. Wu, X. Han, X. Wang, J. Shao and Z. Xia, *J. Biol. Chem.*, 2014, **289**, 24226–24237.

This journal is © The Royal Society of Chemistry 2024